5.4 The form factor

According to Usher & Whitney (1968) the form factor, m introduced as $\rho/\rho_0 = X^{-m}$ is given by

$$m = \frac{\log\left[(X^3 - \eta^3)/(1 - \eta^3)\right]}{\log(X)}, \tag{5.38}$$

where $\eta \equiv R_{\rm c}/R_\star$, being $R_{\rm c}$ the core radius. One can remark the necessary condition $X > \eta$, otherwise the argument of the logarithm becomes negative. Moreover, since $R_{\rm c}$ is considered to be the radius of the rigid core that does not participate to the pulsation, it is also physically meaningless that R reaches values smaller than $R_{\rm c}$. It is worth noting that in none of the several studies existent in the literature regarding this one-zone model (neither radiative nor convective) is Eq.(5.38) used, but its value corresponding to small oscillations ($R \approx R_\star$), that is

$$m_0 = \frac{3}{1 - \eta^3}. \tag{5.39}$$

While the use of Eq.(5.39) avoids the mathematical problem of a negative argument for the logarithm, it does not resolve the unphysical situation of R reaching values smaller than $R_{\rm c}$. As considered also in the previous sections, $m = 10$ is used in Stellingwerf (1986), to which corresponds an $\eta = 0.888$ leading to $R_{\rm min} \approx 0.82$. Therefore, large excursions of X_0 should be considered with caution when using Eq.(5.39).

On the other hand, we argue in favor of not considering the "shell thickness", $(1 - \eta)$ in dimensionless formulation, equal to the range in radius of the envelope. In evolutionary models, the envelope is a structured dynamic entity consisting in a high number of layers playing different roles in the pulsational history of the star. The driving is accounted for indirectly in the sense that, during the evolution of the stellar model, certain layers of the envelope fulfill the conditions for the H and/or He partial ionization and become driving regions. A simplification of the envelope structure should include, from inner to outer regions: a damping region, a driving region, a transition region and the dissipation region. From this point of view, the model of Icke et al. (1992) accounts for a driving region (piston approximation) at $X \approx 0.2 - 0.4$, a transition region through which the pressure waves from the interior propagate, and a dissipation region that they call mantle, where the waves decrease their amplitude. In Stellingwerf (1986), the one-zone model consists in a dissipation region bounded below by a rigid core at $X \approx 0.85$ excited by a driving agent ($\Gamma_1 < 4/3$). Apparently, the two models are incompatible as, if the rigid core is considered at $X \approx 0.85$, no driving can originate at $X \approx 0.4$. However, a consensus can be reached if the concept of *rigid core* boundary of Stellingwerf (1986) is considered as the inner boundary of the dissipation region. In this sense, the idea of "shell thickness" might be equivalent to the radial extension of the dissipation region.

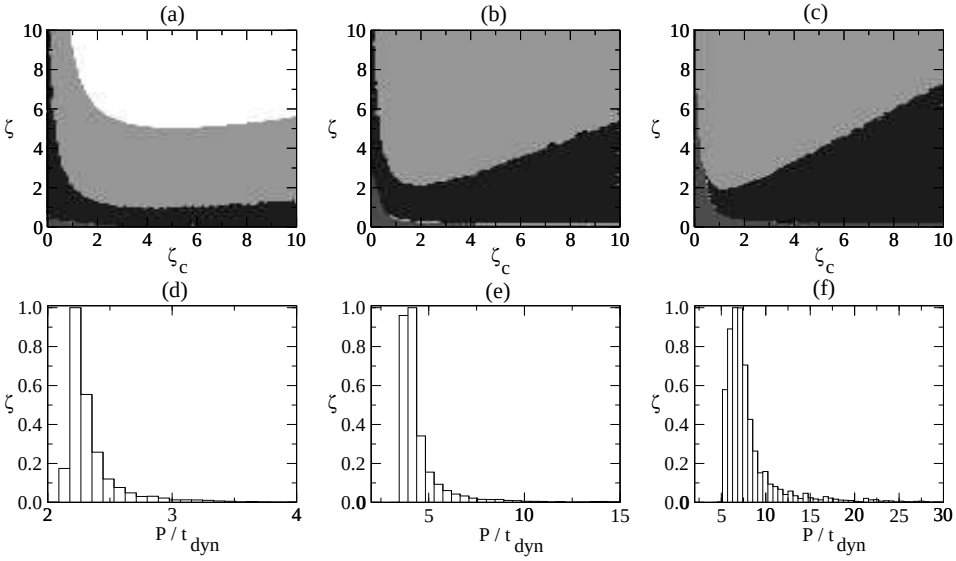

Figure 5.12: Influence of the shell thickness. Locations of the limit cycle regions (in black) as well as stable (light grey), unstable (dark grey) and singularity regions (white regions) in the (ζ, ζ_c) plane for $\gamma_c = 0.4$, $\alpha_p = 0$ and: *(a)* $\eta = 0.888$; *(b)* $\eta = 0.8$; *(c)* $\eta = 0.7$. Eq.(5.38) was used for the form factor. The histograms of the periods for the above cases are presented in *(d)*, *(e)* and *(f)*, respectively.

It is, hence, highly desirable to use Eq.(5.38) in modeling stellar pulsations, because of its more reliable physical meaning. Therefore, we present in this section the results of an analysis similar to the ones already done in §5.1 and §5.2, but which includes the variable nature of the parameter m and the importance of the shell thickness, η. For a better illustration of the importance of the variable form factor, we have investigated first the case of zero-turbulent pressure. In Figure 5.12*a*, *b*, *c*, we plot the plane (ζ, ζ_c) for different values of the shell thickness, η, and for an intermediate degree of convection. One can notice that the increase of the shell thickness produces the increase of the regions characterized by limit-cycle behavior. Moreover, we have noticed that the histogram of the periods for the limit cycles (Figure 5.12*b*) present a clear correlation with the shell thickness. They represent a good approximation of a Poissonian distribution whose maximum corresponds to higher periods for thicker shells. In other words, it is a confirmation of the association of thiner shells to higher overtones: the first (half the fundamental period) and second (a third of the fundamental period) overtones.

We have considered further the changes introduced by the turbulent pressure coupled with the variable form factor. We have chosen to represent in Figure 5.13 the regions of different types of dynamics in the plane (ζ, ζ_c) for the case of $\eta = 0.8$, as being an intermediate case. One can notice that limit cycles exist for higher values of the convective/radiative parameter, γ_c, as a consequence of a thicker shell. On the

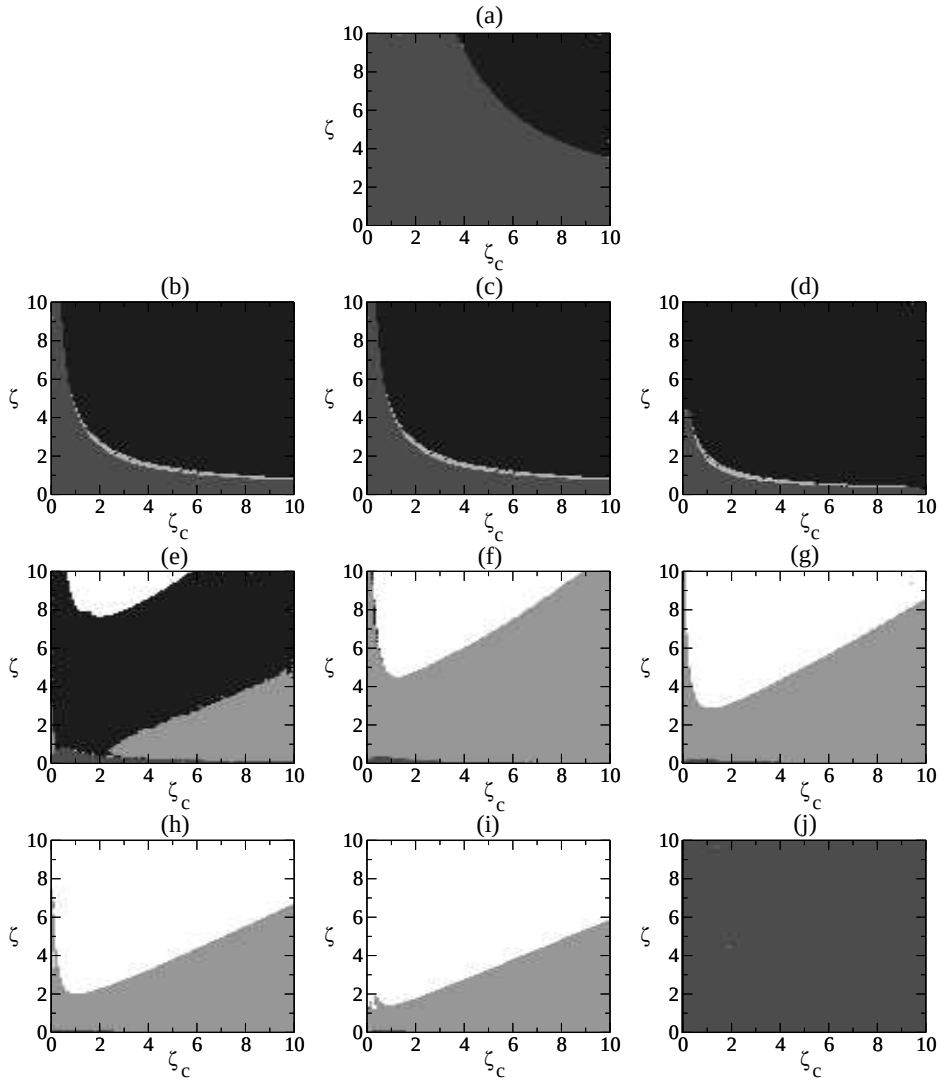

Figure 5.13: Same as Figure 5.7, but for the case in which turbulent pressure and variable form factor are considered ($\eta = 0.8$). The white regions represent the cases leading to singularities.

other hand, the limit-cycle and stable regions existent for the case of $\gamma_c = 1$ with constant form factor disappear with the introduction of the variability of the form factor and the turbulent pressure (Figure 5.13 *j*). More precisely, for the disappearance of the limit-cycle region it suffices the introduction of the variability of the form factor.

The study presented in the last sections was concerned with a mathematical analysis of the model, and it was related mainly to its dynamic behavior. In order to be able to establish any relationship between the results and the observations, a more reliable observational characteristic must be extracted from these results. For this purpose, we present in the next section the study of the limit cycle characteristics.

5.5 Limit cycle characteristics

Unfortunately, in the case of simple models such as the one we are analyzing in the present chapter the task of comparison with observations is tricky and mainly qualitative. For these cases, the best way out of this dilemma is the classification of the light curves morphology by assigning quantitative terms to the shape of the light curves in order to enable reliable comparison with real data. Therefore, we shall analyze the morphology of the luminosity and velocity curves for the limit cycle cases and infer the roles played by the pulsation-convection interaction.

In all the cases presented in the previous sections, the region of limit cycles can be considered as an equivalent of the Cepheids instability strip (red region of the HR diagram in Figure 1.2). First, we shall consider the case in which neither the turbulent pressure nor the variability of the form factor is taken into account. That is, we study the case discussed in §5.2. In Figure 5.14 we summarize the types of light curves encountered when moving from the stable-region border (red-blue border in Figure 5.7) to the unstable-region border (blue-red border in the same Figure). We have chosen to illustrate the case of $\gamma_c = 0.2$ and $\zeta_c = 3$, while ζ was varied from high values to low values in the limit-cycle region. The morphology of Figure 5.14 is generic for all values of γ_c for the model of Stellingwerf (1986) except for $\gamma_c = 1$. In other words, the transition from the stable region to the unstable region through the limit-cycle region follows the sequence of Figure 5.14 for all the values of γ_c. For the case of $\gamma_c = 0.4$ — Figure 5.7*d* — the unstable region is represented by a very small fraction of the (ζ, ζ_c) plane and the transition is not so well represented as in the cases of smaller γ_c. That is, the values of the parameters in the proximity of the blue-red border yield light curves of low period and amplitude (e.g., not pulse-like) as the distance to the green-blue border is too small for the limit cycle to grow significantly in amplitude.

The detailed-zoning nonlinear models reveal that the transition from the red edge (low temperature) to the blue edge (high temperature) of the instability strip implies the increase of the luminosity amplitude until it becomes unstable (Figure 16 of Bono & Stellingwerf 1994 for RR Lyrae and Figure 11 of Bono et al. 2000a for Clas-

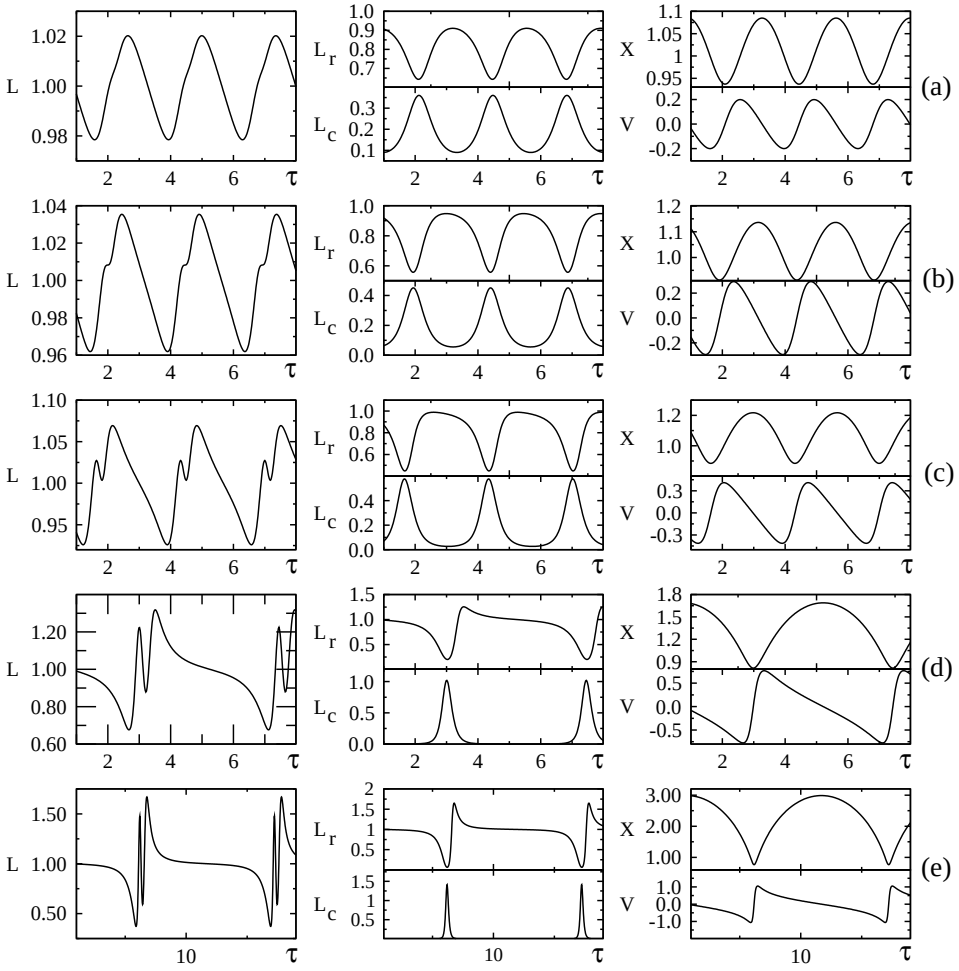

Figure 5.14: Morphology of the light curves for the cases of the model of Stellingwerf (1986), that is with no turbulent pressure and constant form factor. The total luminosity, L *(left panels)*; radiative luminosity, $L_{\rm r}$ and convective luminosity, $L_{\rm c}$ *(middle panels)*; radius, X and velocity, V variations *(right panels)* are shown. The parameters are $\gamma_{\rm c} = 0.2$ and *(a)* Small amplitude: $(\zeta, \zeta_{\rm c}) = (6.5, 3)$; *(b)* Bump Cepheid: $(\zeta, \zeta_{\rm c}) = (5.5, 3)$; *(c)* Double-peak Cepheid: $(\zeta, \zeta_{\rm c}) = (4, 3)$; *(d)* Steep bump: $(\zeta, \zeta_{\rm c}) = (1.5, 3)$; *(e)* Pulse-like: $(\zeta, \zeta_{\rm c}) = (0.7, 3)$.

sical Cepheids). Rewardingly, the observations confirm such a behavior and, more exactly, the light curves of RR Lyrae variable stars in the globular cluster IC 4499 (Figure 2 of Clement et al. 1979) show a remarkable similarity. As far as the periods are concerned, the transition from the red to the blue edge occurs with a continuous decrease in period (Bono & Stellingwerf 1994; Bono et al. 2000a). Apparently, this is in contrast with our results. However, one must take into account that our results have a non-dimensional form. Physically, this covers the fact that for different values of $\gamma_{\rm c}, \zeta$ and $\zeta_{\rm c}$ correspond different normalizing values for the stellar luminosity, radius and dynamical time scale. Unfortunately, for this reason the direct comparison with observations may be misleading.

In Figure 5.14, one can notice that the approach to the unstable region gradually transforms the convective luminosity from a sinusoidal variation to a pulse-like variation and also leads to the appearance of a bump-like feature on the ascending branch of the total luminosity. The bump increases as the period of the light curve increases, but never reaches the height of the main peak which might be considered of radiative origin. The double-peak appearance of the light curves of panels *(b)*, *(c)* and *(d)* makes a clear reference to what are generally called Bump Cepheids and constitute a guaranty that the values of the parameters for these cases are definitely within the instability strip. The pulse-like cases (panel *e*) appear for values of $(\zeta, \zeta_{\rm c})$ close or on the frontier with the unstable region. In spite of the existence of a limit cycle in such cases, they should not be considered as part of the instability strip as no such steep light curves have been observed yet.

Generally, the main effect of convection when moving to lower temperatures within the instability strip is to increase the fraction of the period over which convection carries a large amount of the total flux. In the present model, it translates into higher values of $\gamma_{\rm c}$ and $\zeta_{\rm c}$. Another simplification of the present model is the constancy of the time-scales ratios, ζ and $\zeta_{\rm c}$, over the pulsation cycle. These parameters normally vary during the pulsation, with convection being more efficient (small convective time scale and, thus, $\zeta_{\rm c}$ large) near minimum radius and with the H- and He-ionization regions alternating the efficiency of the convection in the envelope.

The variability of the form factor, m, enriches the morphology of the light curves, as can be seen in Figure 5.15. Compared to the case of constant form factor, the bump introduced by the convective luminosity in the light curve gains more strength when the form factor is allowed to vary according to Eq.(5.38). Additionally, for certain values of $(\zeta, \zeta_{\rm c})$, it becomes the main maximum in the light curve (Figure 5.15*b, c, d, e*). More exactly, approaching the unstable region through the limit-cycle region, the light curve acquires a double-peak form, with the first peak gaining more and more amplitude with respect to the second one.

The introduction of the variable form factor leads to a light-curve morphology which reminds the so-called Hertzsprung Progression (HP) of the Bump Cepheids of periods $6 < P < 16$ days (Bono et al. 2000b). The HP consists in a bump along both light and velocity curves and appears on the descending branch for Cepheids with periods up to 9 days, close to the maximum light for $9 < P < 12$ days and on

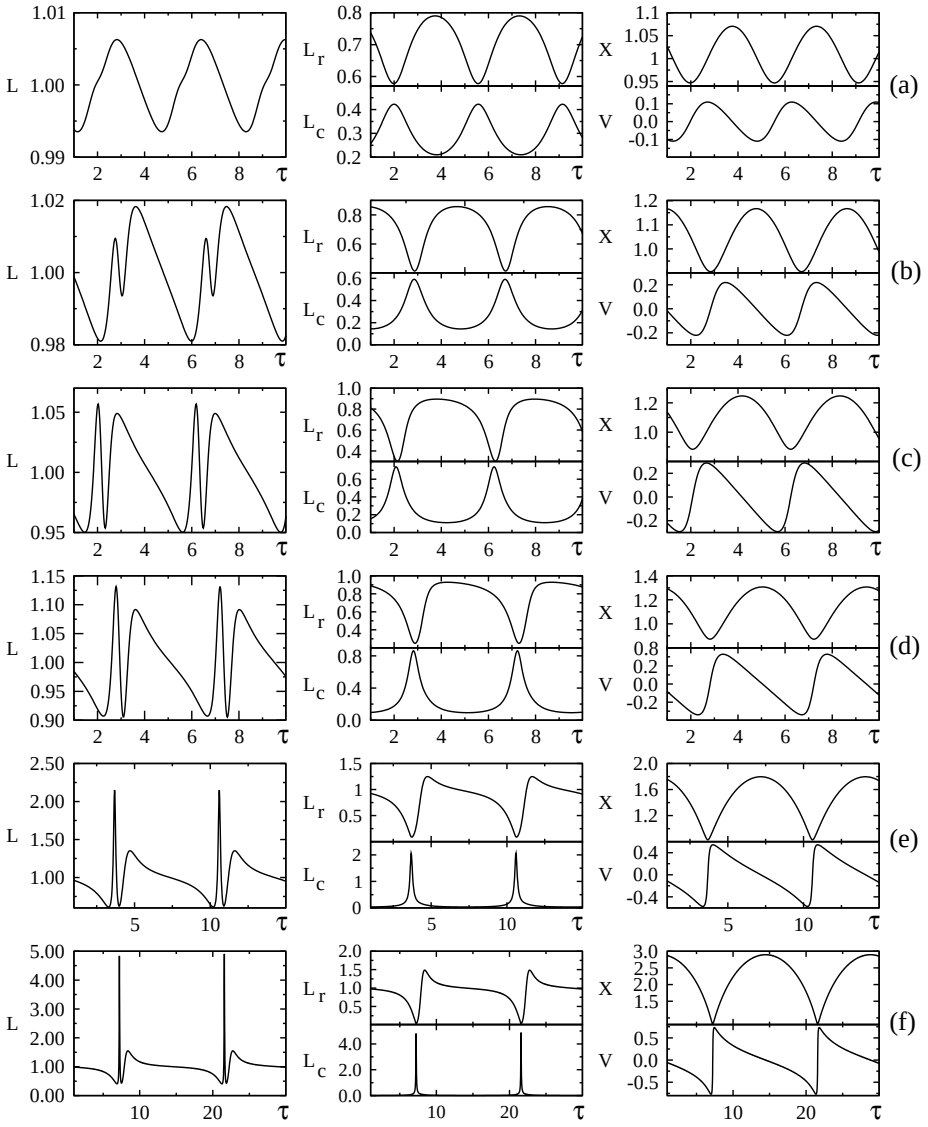

Figure 5.15: Morphology of the light curves for the cases of the model of Stellingwerf (1986) with variable form factor: total luminosity *(left panels)*; radiative luminosity, $L_{\rm r}$, and convective luminosity, $L_{\rm c}$, *(middle panels)*; radius, X and velocity, V variations *(right panels)*. The parameters are $\gamma_{\rm c} = 0.3$ and *(a)* Small amplitude: $(\zeta, \zeta_c) = (8.5, 9)$; *(b)* Bump Cepheid: $(\zeta, \zeta_{\rm c}) = (6, 9)$; *(c)* Double-peak Cepheid: $(\zeta, \zeta_{\rm c}) = (3, 9)$; *(d)* Lowest minimum Double-peak: $(\zeta, \zeta_{\rm c}) = (1.8, 9)$; *(e)* Steep bump: $(\zeta, \zeta_{\rm c}) = (0.8, 9)$; *(f)* Pulse-like: $(\zeta, \zeta_{\rm c}) = (0.3, 9)$.

the ascending branch for longer periods. In our case, the bump appears only on the light curve. Moreover, for a fixed γ_c, the bump appears on the rising branch for small periods and it becomes the main maximum for longer periods with the previous maximum being now a peak on the descending branch. At a first glance, one might say that a reverse HP is observed: that is, with a bump on the ascending branch for *short periods*. However, it is misleading to consider a straightforward comparison within a case of constant γ_c as it is clear that along the real HP, the importance and efficiency of the convection varies, and therefore the HP implies also a variation in at least γ_c and ζ_c.

Besides this visual (and quick) analysis, a more quantitative parameterization of the light curves might help in the comparison. The quantities generally used to describe the shape of the light curves are the skewness and the acuteness (Stellingwerf & Donohoe 1987). They are inspired by the sawtooth appearance of the light curves of Cepheids and RR Lyrae variables (the rising branch of the light curve is shorter than the descending branch). An example of such an asymmetric Cepheid-like light curve is shown in Figure 5.8. The skewness, S, is defined as the ratio of the phase duration of the descending branch to that of the rising branch, while the acuteness, A, is given by the ratio of the phase duration of the lower-than-average light to that of the greater-than-average light. The work of Petersen (1984) on the RR Lyrae stars in the ω Centauri globular cluster revealed a skewness in the range of $S \in [0.25, 6]$. Within this interval, Stellingwerf & Donohoe (1987) used the model of Stellingwerf (1972) to estimate the acuteness, A, which resulted to belong to the interval $A \in [1, 2.5]$ for values of S greater than 1. Under these guidelines we performed a detailed study of the morphology of limit-cycle cases and of the effect of the turbulent pressure and variable form factor on the skewness and acuteness.

In the left panels of Figure 5.16 we plot the acuteness versus skewness for the case of constant form factor $m = 10$, whereas in the middle panels we show the case of variable form factor ($\eta = 0.8$). In both cases, skewness values higher than approximatively $S > 8$ imply pulse-like behavior similar to those of Figure 5.14*e* and Figure 5.15*f*. Note that in Figure 5.16- *middle panels*, a lower limit was chosen for the representation in order to better visualize the three groups mentioned above. While the constant-m case leads to more compact and restricted regions in the (A, S) plane, the case of variable m yields three distinct regions which become more separated as γ_c increases: a group of $S \approx 0$, one whose S is centered on reasonable values increasing as γ_c decreases, and another group of very high values of S. Moreover, for the case of variable m, the skewness reaches extreme values ($S = 350$ for $\gamma_c = 0.1$) which slightly decrease as γ_c increases. Among these groups, the extremes ones (very low and very high skewness values) represent the convective-maximum cases, with very low skewness for cases such as the one of Figure 5.15*d* and high or extreme values of skewness for cases similar to Figure 5.15*c, e, f*. The middle group — best seen in the middle panel of Figure 5.16*d,e*— represents the radiative-maximum cases, such as Figure 5.15*b*. These groups appear well identified in the (ζ, ζ_c) plane of the right panels of Figure 5.16. There, the radiative-maximum cases

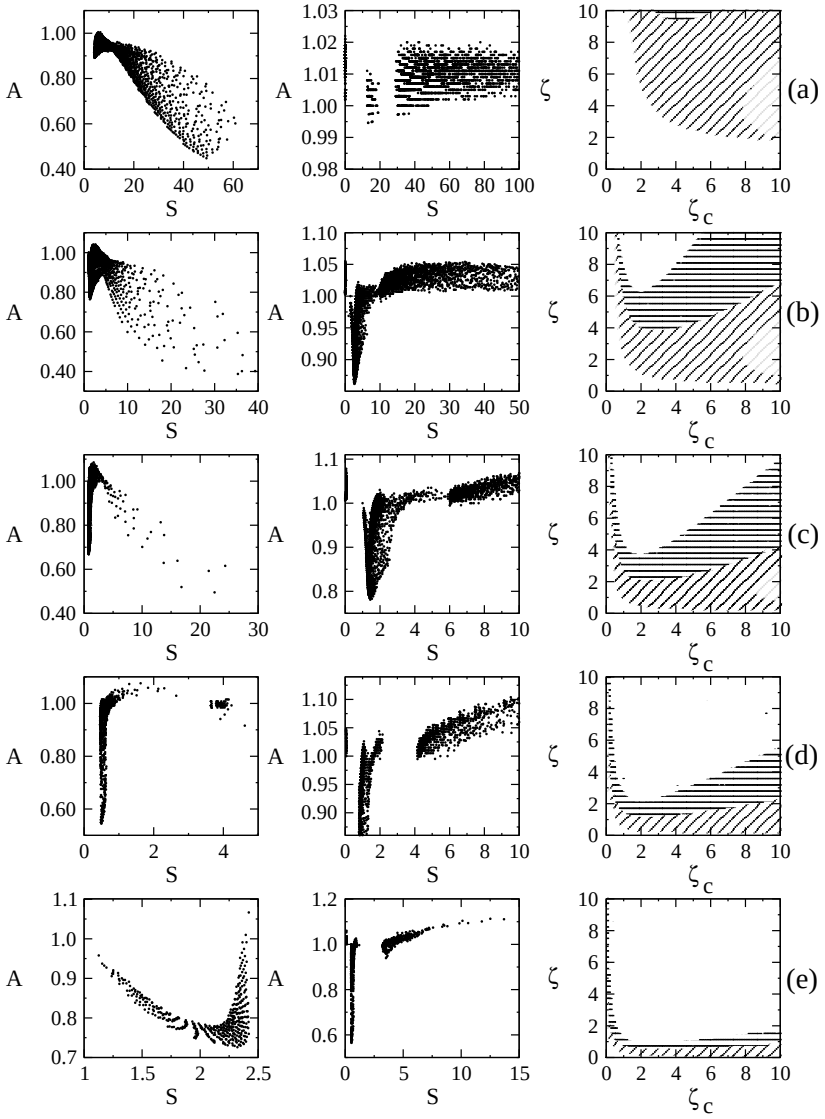

Figure 5.16: Acuteness versus skewness for constant form factor *(left panels)* and variable form factor *(middle panels)* and the limit-cycle regions in the (ζ, ζ_c) plane *(right panels)* for the latter case distinguishing radiative-maximum cases *(horizontal dashed region)* from convective-maximum cases *(inclined-dashed regions)*. *(a)* $\gamma_c = 0.1$; *(b)* $\gamma_c = 0.2$; *(c)* $\gamma_c = 0.3$;*(d)* $\gamma_c = 0.4$; *(e)* $\gamma_c = 1.0$ *(left panel)* and $\gamma_c = 0.5$ *(middle panel)*.

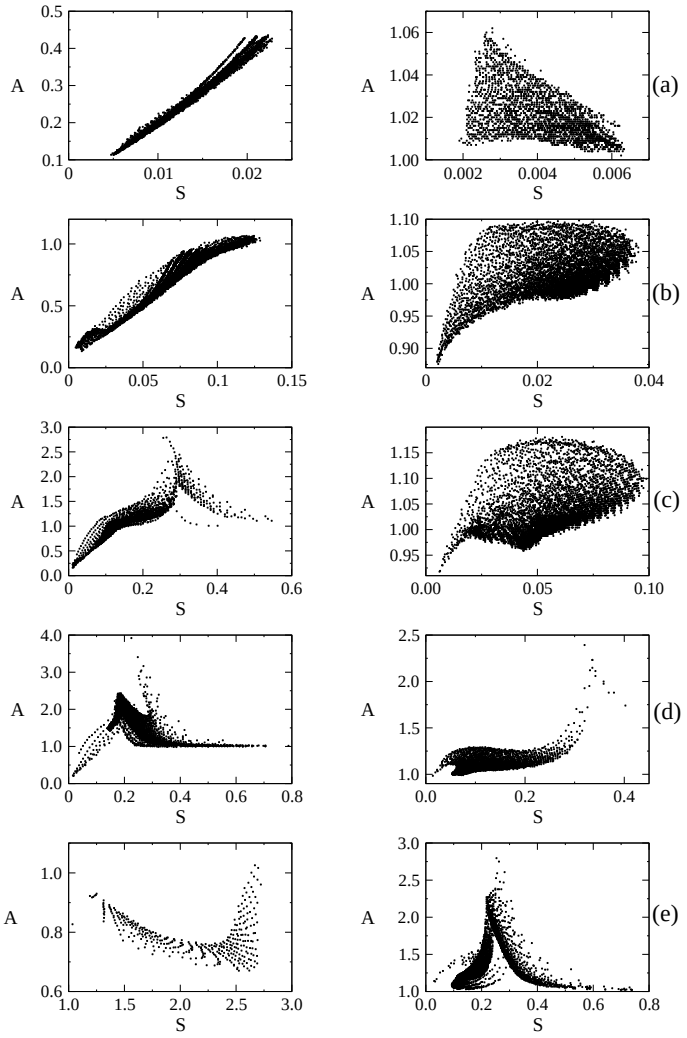

Figure 5.17: Acuteness versus skewness for constant form factor *(left panels)* and variable form factor *(right panels)* considering the turbulent pressure. *(a)* $\gamma_c = 0.1$; *(b)* $\gamma_c = 0.2$; *(c)* $\gamma_c = 0.3$;*(d)* $\gamma_c = 0.4$; *(e)* $\gamma_c = 1.0$ *(left panel)* and $\gamma_c = 0.5$ *(right panel)*.

appear as horizontal-dashed regions, while the convective-maximum cases are represented as inclined-dashed regions, with the grey dashed regions being the cases when the minimum of the light curves follows immediately the convective maximum (e.g. Figure 5.15*d*). The convective cases appear as a direct consequence of the variability of the form factor, as no such examples exist for m constant.

The price payed for the enriched morphology is the dissappearance of the limit-cycle regions for the completely convective case ($\gamma_c = 1.0$). The results shown in Fig-

ure 5.16 were intended to verify the remark expressed in §5.4 that thicker shells lead to the existence of limit cycles for higher values of γ_c (Figure 5.13*e*). In Figure 5.16 we confirmed this remark as for the case of constant $m = 10$ with $\eta = 0.888$ the existence of limit cycles is limited to $\gamma_c < 0.5$, while for variable m with $\eta = 0.8$, limit cycles exist even for $\gamma_c = 0.5$. We have also verified that for the case of variable m with $\eta = 0.888$, no limit-cycle region appears in (ζ, ζ_c) plane with $\zeta, \zeta_c \in [0, 10]$ and $\gamma_c = 1$. As a general remark related to all cases of γ_c, it is not excluded that limit cycles exist for higher values of ζ and ζ_c than the one considered in this study. Indeed, during a substantial fraction of the pulsation phase for the models of RR Lyrae of Bono & Stellingwerf (1994), ζ_c remains in the vicinity of 10 (their t_h/P close to 0.1, being t_h the convective timescale of hydrogen shell). It should be even more important for the completely convective case for which a more efficient convective transport is expected and, accordingly, $\zeta_c > 10$. One can see both in Figure 5.7*j* and in Figure 5.11*j* that only a very small fraction of the limit-cycle region is encompassed by $\zeta, \zeta_c < 10$ and that it extends substantially for higher values.

A drastic change in the morphology of the light curves is caused by the introduction of the turbulent pressure. In Figure 5.17, we plot the acuteness versus skewness when the turbulent pressure is taken into consideration, both with and without the variability of the form factor. All cases present the characteristics of the group of very small skewness found in the previous study on the influence of variable form factor(Figure 5.16*c, d, e*). From the former and the latter figure, one should expect a light curve of the type drawn in Figure 5.15*d*, more precisely, a maximum immediately followed by the minimum. We have verified this statement and as an example, we represent the typical light curve for the cases of Figure 5.17 in Figure 5.18*a*. For all these cases, as can be seen also in Figure 5.11 and Figure 5.13, the stable, unstable and limit-cycle regions are located in such a way in the (ζ, ζ_c) plane that no clear transition from the stable to the unstable regions through the limit-cycle region can be performed. However, it can be noticed a tendency to decrease the amplitude and period of light-curves further away from the unstable region. All the examples of Figure 5.18 share the characteristic feature consisting in a bump preceeding the maximum, which becomes flatter with longer periods (panels *b,c,d*. We stress the fact that no evolution of the morphology exists with the values of the parameters and that the limit cycles are homologous to the ones of Figure 5.18.

A particularity undoubtly due to the turbulent pressure is the high values of acuteness reached for cases such as $\gamma_c = 0.3$ and $\gamma_c = 0.4$ for constant form factor and $\gamma_c = 0.4$ and $\gamma_c = 0.5$ for the case of variable m and thicker shell (Figure 5.17). We have chosen to represent in Figure 5.18 also two cases of high acuteness (panels *b* and *c*) characterized both by $(S, A) \approx (0.32, 2.4)$ for $\gamma_c = 0.4$. As expected from the definition of acuteness, one can see that the light curves are characterized by a long duration of lower-than-average luminosity and by an incipient pulse-like feature which increases in amplitude with the increase in period (panel *d*).

From the previous figures we can also draw the conclusion that the turbulent pressure has more impact on the morphology of the light curves than the variable

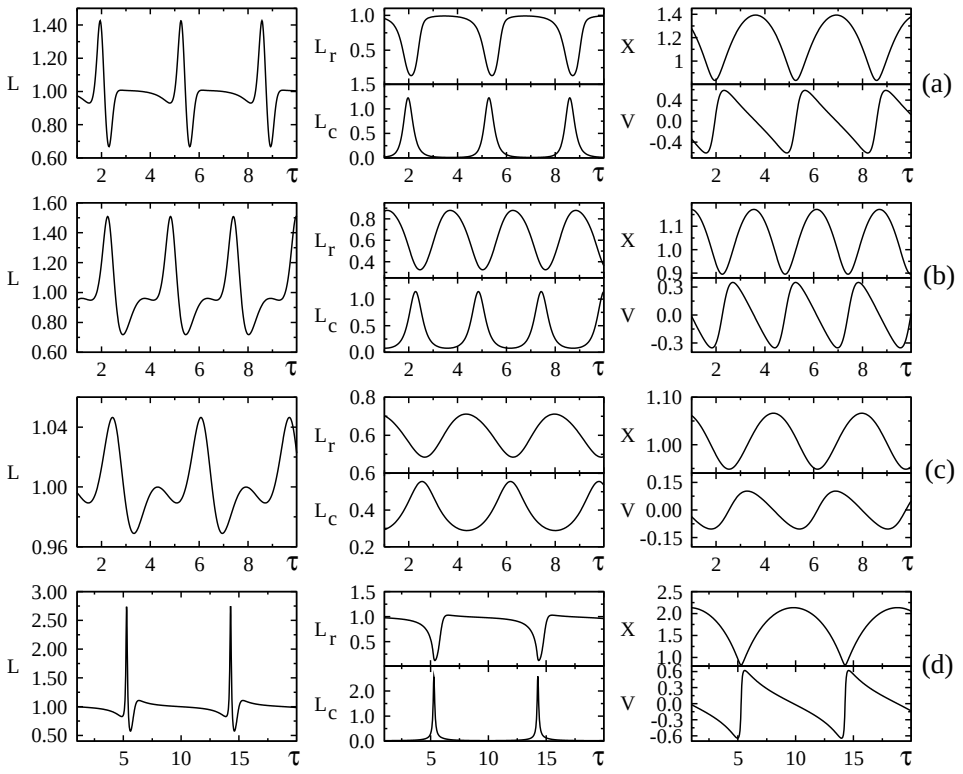

Figure 5.18: The characteristic limit cycle with constant m when turbulent pressure is taken into account: *(a)* $\gamma_{\rm c} = 0.3$ and $\zeta = \zeta_{\rm c} = 2$; *(b)* $\gamma_{\rm c} = 0.4$, $\zeta = 0.4$, $\zeta_{\rm c} = 4.7$; and with variable m: *(c)* $\gamma_{\rm c} = 0.4$, $\zeta = 0.4$, $\zeta_{\rm c} = 9.9$; *(d)* $\gamma_{\rm c} = 0.3$, $\zeta = 0.9$, $\zeta_{\rm c} = 5.1$. The quantities are total luminosity, L, radiative luminosity, $L_{\rm r}$, convective luminosity, $L_{\rm c}$, radius, X and velocity, V.

form factor in the sense that the introduction of the turbulent pressure cancels the effect of the variable form factor whose influence on the limit-cycle characteristics led to the progression illustrated in Figure 5.15. More precisely, the comparison with observations should be considered only for the case of variable m and without turbulent pressure. On the other hand, for the present study only the value of $\alpha_{\rm p} \approx 0.4$ of the fraction of the pressure due to turbulent pressure, was considered. Such a significant contribution was used in order to clearly identify the impact of the turbulent pressure. However, it would be interesting to investigate if lower values of $\alpha_{\rm p}$ might provide only mild changes of the morphology. We remark here also that the initial values have a crucial influence on the value of $\alpha_{\rm p}$, but are obviously not remembered in the final limit-cycle. In this sense, studies such as those of Stellingwerf & Donohoe (1986) and Stellingwerf et al. (1987) concerning the evolution of the morphology of the limit cycles with the initial conditions (e.g. radius) are somewhat puzzling.

5.6 Discussion

The study of the convection in simple models of stellar pulsations was initiated as a natural step in the series of investigations presented in the previous chapters and also as a consequence of some oversights encountered in a convective one-zone model existent in the literature (Stellingwerf 1986). This model and simplified versions of it have been the object of several other papers (Stellingwerf & Donohoe 1986, 1987; Stellingwerf et al. 1987; Stellingwerf & Gautschy 1988). The main characteristic of these studies that drew our attention was the detailed analysis of the light curve morphology and the subsequent comparison with real data for cases in which the parameters chosen did not provide a limit cycle. We consider crucial the existence of a limit cycle as any unstable solution is not expected to be seen in nature. Therefore, in this study we performed a thorough search for the regions in the space of parameters leading to a limit-cycle behavior. Rewardingly, we encountered regions of limit cycles and for these cases, we studied the morphology of the light curves. Moreover, we extended the model by including the turbulent pressure and geometric considerations. For these cases, we searched also for the limit cycle behavior and investigated the light curve morphology. The geometric considerations included the variability of the form factor, m, which has not been considered in any of the previously-studied related models. The results provided an interesting progression of the light curves with the period, as well as a richer morphology than the case of constant form factor. In the end, the case of variable form factor and no turbulent pressure resulted to resemble better the observational data.

Chapter 6

Conclusions

Nowadays, the physical processes responsible for the pulsation mechanism are well understood individually (driving mechanisms, convection, turbulence, shocks). However, the emergent properties resulting from the simultaneous action of these processes as well as the lack of transparency of the mathematical aspects of the equations governing these processes are the cause of the development of simple models. This approach is justified by the search of a more tractable mathematical and physical methodology in order to better understand the morphology of the light curves of variable stars. In the last decades, the formalism of dynamical systems theory including both hamiltonian and dissipative systems has been widely used to explore the presence of nonlinear phenomena in astrophysics (Covas 1995). The approach adopted in this thesis is not intended to be a substitute for finely zoned nonlinear calculations such as the numerical hydrodynamical codes (Höfner 1999; Bono et al. 2000b; Simis 2001). The results obtained using one-zone models are qualitative and therefore quantitative agreement with the observations might be meaningless. Therefore, in these conclusive remarks concerning our work we shall concentrate only on the general aspects and implications that can be extracted from it.

In the first part of our work synthesized in Chapter 3, we have presented and analyzed the dynamics of a forced oscillator which resulted interesting not only as a model on its own right embodying the essentials of adiabatic stellar oscillations, but also because of its fascinating mathematical features. This model has been previously used to study the irregular pulsations of low mass stars on the Asymptotic Giant Branch — AGB (Icke et al. 1992), and we have extended this study to a range of values of the parameters typical of more massive and luminous pulsating stars, the Super-Asymptotic Giant Branch (SAGB) stars. In the model, the driving was characterized by two parameters, the fractional amplitude of the internal perturbation, α and the total amplitude of the driving, ϵ. The evolutionary status of the star was contained in the parameter ω, a measure of the core–envelope ratio providing information on the location of the driving source. The general aspects and results of our study made the object of an article in a journal of broad mathematical and physical interest (Munteanu et al. 2002), while the detailed mathematical explanation of such

a rich dynamics was included elsewhere (Munteanu et al. 2003c).

As the oscillator is characterized by a time-periodic forcing, our main object of analysis was the Poincaré (stroboscopic) map associated to the system. The parametric study yielded a rich set of local and global bifurcations. Among these, maybe the most important one is the triplication bifurcation. We have shown that for a given total amplitude of the driving, $\epsilon > 0$ there exists a value of the fractional amplitude, $\alpha^*(\epsilon)$ that corresponds to a triplication of the central elliptic fixed point of the Poincaré map. According to Dullin et al. (2000), this implies that the Poincaré map acquires a nontwist character and a twistless bifurcation occurs or, equivalently, the rotation number as a function of the distance from the elliptic fixed point becomes a nonmonotonic function. As we were interested in values of the parameters α and ϵ above the triplication curve, the nontwist character of the map was undoubtedly present. We have argued that due to both the acquired nontwist character and the periodic character of the perturbation, the map presents the typical features of a generic class of nontwist area preserving maps, such as reconnection and meandering, with the nongeneric scenario of creation of vortices. The nonmonotonic property due to the triplication bifurcation is shown to be different from that exhibited by the cubic Hénon map, which can be considered as the prototype of area preserving maps which undergo a triplication followed by the twistless bifurcation. Moreover, we have noticed that the richness of the dynamics is due mainly to ω being a rational number and not a natural number. The probability that ω, which is a measure of the core/envelope ratio, is a rational rather than a natural is extremely high and this gives more validity to the conclusions that might be extracted from the dynamics of the model concerning the stellar variability.

Concerning other bifurcations in the dynamics of the system, special attention was devoted to the process of formation of periodic orbits and to the collision of periodic orbits. Using these elements, we have followed the sequence of local and global bifurcations until the formation of stochastic layers around separatrices together with the associated sticky orbits. We have proved that the reconnection of even periodic orbits is generic by following the reconnection of two Poincaré-Birkhoff chains of period 34.

From the astrophysical point of view, a first look at the phase space of the system in the case of an AGB and of a SAGB star model (different ω, fixed α and ϵ) revealed that the regions occupied by the chaotic sea were more extended in the SAGB-case. This is in agreement with the observations of Long Period Variables (LPV) which are the observational counterparts of the pulsating SAGB stars. The richness of the Poincaré map translates into a high variety of time series. For example, we have shown that although there are light curves which show a rather typical regular behavior for certain values of the parameters of the system and given initial conditions, there are as well some other regular cases which show clear beatings or linear combinations of two main frequencies up to terms of $2f_0$+$7f_1$, being f_0 the fundamental frequency and f_1, the first overtone. For values of the parameters and initial conditions leading to irregular behavior, we noticed the existence of both clear chaotic

pulsations and sudden changes from regular to chaotic pulsations, the latter being associated to the sticky orbits characteristic of hamiltonian systems. For the chaotic orbits, the velocity of the outer layers exceeds the escape velocity and thus mass loss is very likely to occur, in good agreement with observations which correlate the degree of irregularity with the mass-loss rate. Regarding the stickiness property, it is worth remarking that the long-term effects found in real stars are reproduced by our model, even though the driven oscillator does not incorporate the effects of secular changes. Hence it may be possible that this kind of behavior already found in full hydrodynamical simulations (Ya'ari & Tuchman 1996) is intrinsically associated to the physical characteristics of the stellar oscillations and not to the long-term thermal changes.

We have dwelled constantly on the necessity of considering the nonadiabaticity as a crucial feature in modeling pulsating stars. In practice, we explored the implications of nonadiabaticity through a one-zone model described and analyzed in Chapter 4. As in Chapter 3, the oscillator was driven by sinusoidal pressure waves and the driving was characterized by the fractional amplitude of the internal perturbation, α and the coefficient of transmission of the pressure waves through the envelope, Q. Our model is an extension of the models proposed by Icke et al. (1992) and Saitou et al. (1989). In particular, Icke et al. (1992) proposed an adiabatic model driven by pressure waves (the piston approximation) whereas Saitou et al. (1989) studied a simple nonadiabatic model without driving (the self-excited pulsation model). We have explored the interesting particularities of the system both from the astrophysical and from the mathematical point of view. We have found that the degree of nonadiabaticity is a determining factor in the development of the period-doubling route to chaos, in particular the period-doubling sequence develops with the increase of nonadiabaticity.

The saturation of the κ-mechanism in the stellar envelopes appears to be a valid candidate for yielding the period-doubling route to chaos. Moreover, coupled with the interior driving, results into a peculiar dynamics similar to that found for some Mira stars. In Chapter 4, we stressed the particularities introduced in the dynamics of the system by the time-dependent perturbation. Namely, a consequence of increasing the parameter Q while α is kept fixed is the creation of a knot-like structure in the space defined by the stroboscopic map of the variables (r, v, p). Our results revealed that the critical phenomenon occurs for a certain range of the strength of the perturbation, that is for certain pairs of (Q, α). Therefore, to a fixed value of α corresponds a sequence of values of the parameter Q at which additional loops are born. More exactly, for other values of the fixed parameter α together with the associated sequence of Q-values, the resultant dynamics is equivalent to the one portrayed in Chapter 4, including the temporal characteristics. More precisely, we have also noticed that for increasing strengths of the pertubation new loops are created. At high values of the strength of the perturbation within the range yielding the knot-like structure, the behavior changes: the creation of new loops stops.

The assumption of radiative transfer provides a simple and compact formula

for the stellar luminosity, which allows a quick visual comparison with real stellar variability data. The light curves are characterized by a repetitive pattern consisting in a major peak followed by n minor peaks, where n is the number of loops in the Poincaré map. In other words, the creation of a new loop represents a new peak in the light curve. As previously mentioned, we have noticed that for increasing strengths of the perturbation new loops are created and the time interval between major bursts increases reaching time intervals of the order of a thousand years. The resulting light curves show a time interval during which the luminosity preceding every major peak remains constant. This interval increases with Q as well. This makes a clear reference to the periodicities observed in the circumstellar shells of some planetary nebulae and then a causal connection between our results and such observations is enticing.

The values of the input parameters as well as the resultant periodicities assure us that we deal with a simple model of pulsations of LPV stars. Our search in the existent literature yielded several Mira stars having light curves reasonably similar to ours. The pattern of alternating major peaks followed by various minors peaks in the light curve of the prototype of the Mira stars, o Ceti, offers the closest resemblance with our results. Moreover, we relate our results also with the light curves of some peculiar Miras which appear to have double maxima due to alternating deep and shallow minima. Among them, we mention R Cen, R Nor, U CMi, RZ Cyg, and RU Cyg.

We have found as well that the system with internal driving presents both regular and irregular bursting regimes. A regular regime consists in strict periodicity of the major-and-minor-peaks structure as well as in a constancy in the amplitude of each peak. In the stroboscopic map, this translates into a precise loop, while for the system of time-averaged perturbation this implies the existence of an attracting periodic orbit. On the contrary, the irregular regime appears to be characterized by a slight dispersion both in the amplitudes and in the periodicities of the peaks, and thus the stroboscopic map presents fuzzy knot-like structures. In particular, the transition from a regular regime with n loops to another regular regime of $n + 1$ occurs through an irregular regime. We conjectured that this transition occurs through a period-doubling regime. Due to the complicated form of the perturbation, we found no methods — neither analytical nor numerical — for solving this conjecture. Thus, we have only illustrated the period-doubling sequence through the return map of the major peaks of the luminosities. For the cases of irregular light curves a certain similarity can be found with the mode-switching semiregular variable R Dor, in which alternating large-amplitude, long-period Mira-like oscillations and low-amplitude, short-period oscillations apparently occur (Bedding et al. 1998).

We have also obtained a theoretical period-luminosity relationship and compared it with the observational data of Miras in the Large Magellanic Cloud (Feast et al. 1989). In particular, we have focused on those peculiar Miras with long periods which are known to be over-luminous with respect to the best fit of Feast et al. (1989). We have found that our model not only provides a reasonable fit to the period-luminosity relationship of these stars but, additionally, it shows the same

clustering in the period-luminosity diagram as the real data. The ultimate reason for this clustering is closely related to the creation of a new loop in the stroboscopic map, and, consequently, of a new luminosity peak in the corresponding time series. Finally, we would like to stress that although our very simple model succeeds in furnishing reasonable comparisons with real stellar variability data, we consider that more efforts are still necessary for a better understanding of the mathematical implications of its dynamics.

There is a series of caveats that must be mentioned in this conclusive part. Some Mira stars are suspected to have at least two frequencies (Mantegazza 1996) which may vary independently, suggesting that more than one mode is involved. Clearly, one-zone models are unable to reproduce this behavior and this is one of their limitations. Nevertheless, the majority of Miras do not show this behavior. An interesting compromise would be to use the modal coupling. However, although this approach has been used to model the pulsation of Miras (Buchler & Goupil 1988), it is more appropriate for classical Cepheids, RR Lyrae and W Vir stars — see Buchler (1993) and references therein. It is also worth noting here that the piston approximation — first introduced by Bowen (1988) — has been used since then by several authors also in hydrodynamical codes (Fleischer et al. 1995; Höfner et al. 2003) even if it has never been deeply scrutinized for validity. Nevertheless this approximation appears to correctly reproduce the velocities and mass loss rates typical of AGB stars. Hence, it can be regarded as a reasonable first-order approximation of the dynamical effect of the pulsation on the atmosphere. Finally, some of the results concerning this weakly nonadiabatic one-zone model were included in Munteanu et al. (2003b) which was preceeded by a preliminary report (Munteanu et al. 2003a).

From the huge amount of work existent in the literature on stellar pulsations it has become rather clear that purely radiative models are not capable of producing a reasonable agreement with observations (Buchler 1998) and that a feedback between pulsation and convection is needed if more progress is to be made. Convection is the dominant factor that controls the pulsational instability in red stars and also no good interpretation can be made for the red edge of the Cepheid instability strip if the coupling between convection and pulsation is not taken into consideration (Xiong et al. 1998b). In the search of a simple, but physically and mathematically robust recipe for the description of convection we have chosen the theory exposed in Stellingwerf (1982) together with the one-zone model introduced in Stellingwerf (1986). Our simulations of this model revealed several conceptual inadvertences in Stellingwerf (1986). Therefore, we considered necessary to disentangle the causes of the previously-mentioned oversights. Our study of this model has made the object of Chapter 5, where caveats and new results concerning the work of Stellingwerf (1986) were included. The model is an extension of the work from Stellingwerf (1972), aimed to include the effects of convection. It is a typical one-zone model, in the sense of the description used until now, where the shell thickness is defined through the ratio η of the core radius to the stellar radius. The model appears in the form of a system of 4 ODEs where the variables are the radius and velocity of the shell, its

pressure and convective velocity. The nonadiabaticity resides in the pressure which is considered as a nonadiabatic perturbation of the reference pressure and, thus, can be regarded as a nonadiabatic variable of the system. The model accounts for the pulsation through self-excitation in a similar way as the model of Saitou et al. (1989), that is by allowing a value close to unity for the adiabatic exponent Γ_1. The main parameters of the system are the fraction γ_c of convective luminosity with respect to the total luminosity, and time-scales ratios, ζ and ζ_c, which are a measure of the dynamical time scale to the thermal time scale and to the convective time scale, respectively.

The first result of the previous works related to this model or to simplified versions of it that intrigued us was the detailed analysis of the morphology of the resulting light curves for cases in which no limit cycle existed and the solution was either stable (damped amplitude) or unstable (growing amplitude). Since only the cases of limit cycles are expected to be seen in nature, we reason that a parametric study is compulsory to the reliable comparison with observations through identified cases of limit cycles. For this purpose, we have selected a parametric space given by $\gamma_c \in [0,1]$, ζ and $\zeta_c \in [0,10]$. Our parametric study revealed well delimited regions in the parametric space where limit cycles exist. In §5.2 we have described the Hopf bifurcation as one mechanism of limit-cycle creation and identified the soft self-excited nature of the resultant oscillations.

Our results showed a complete disappearance of the limit-cycle regions for cases in which the convection becomes dominant ($\gamma_c \lessapprox 0.5$). As discussed in Chapter 1, the more efficient transport of energy by convection can disable the $\kappa-$ and γ-mechanism of excitation as it can transport away some of the heat trapped at minimum radius and thus quench the pulsations. This onset of efficient convective transfer is thought to be the mechanism determining the red edge of the Cepheid instability strip. Moving from the blue edge to the red edge within the instability strip, convection increases the fraction of the period over which it carries a large amount of the total flux to the detriment of the radiation. In the present model, it translates into higher values of γ_c and ζ_c and explains the disappearance of the limit-cycle region in the vicinity of $\gamma_c \approx 0.5$ depending on the shell thickness.

Not without a certain surprise we found that a limit-cycle region appears in the case of completely convective shell. Even if there is general agreement within the astrophysical community that the intrinsic reason for the existence of the red edge of Cepheid instability strip is the damping produced by convection, there are results suggesting the existence of convection-induced oscillations (Wood 2000). When the convective time scale is much longer than the dynamical time scale ($\zeta_c \ll 1$), the effect of convection is stabilizing, but when the convective time scale is much shorter, the reverse is true (Gough 1967). Thus, it may provide an important driving mechanism in red giants and supergiants. Even if there are no clear models providing undisputed evidence for such a behavior, there are puzzling observational data which are not contrasted by models. Among these, we mention the red variables encountered by Yao et al. (1993) in globular clusters, some of them located outside the RR Lyrae instability strip, and others at the tip of and at the lower middle part

of the RGB, but leftward of the region of the LPV. Even more interesting is the still-unexplained period-luminosity law for LPV (Wood et al. 1999) for which a convective prolongation of the period might be speculated on the roots of our results.

It may also be envisioned that the radiative damping in the deep interior of a star can be largely weakened and may result in increased pulsational instability when the coupling between convection and oscillations is introduced as the excitation regions may extend deeper into the stellar interior. A Mira instability strip shows up outside the Cepheid instability strip when the coupling is considered. For luminous red stars, the convective efficiency parameter, $\zeta_{\rm c}$ is expected to be greater than unity in the interior of the envelope model except for the extremely outermost layer where it may take higher values (Xiong et al. 1998a). However, the internal distribution of the luminous red giants is very different from that of Classical Cepheids (and RR Lyrae) and the former are gravitationally weakly bound compared to the latter (Feuchtinger 1999). In another perspective, the former have a very low mass-luminosity ratios and, therefore, their internal structure has very high central concentration. They have very low envelope mass resulting from the high luminosity blowing out the matter at large radii. The low effective temperature provides high opacity and thus, strong convection is expected (Cox & Ostlie 1993). Theoretically, their study is hampered by the difficulty in dealing with the extended and deep convective envelopes. Under these circumstances, it appears plausible enough that for low temperature stars, both Cepheids and LPV, the partial ionization regions are the source of both convection and pulsational driving, and our results from the one-zone approach may provide some support for such a hypothesis. Considering the remarks expressed above, we might regard the limit-cycle cases of $\gamma_{\rm c} = 1$ as more similar to the RGB pulsators than the AGB pulsators.

Another caveat concerning the model of Stellingwerf (1986) was related to the geometric considerations, more precisely to the simplified formula of the form factor. The form factor introduced by Usher & Whitney (1968) was supposed to account for the existence of the stellar core which does not participate of the pulsations, but which indeed affects the oscillations by assuring a strong rebound when the shell radius reaches the core radius. The *rigid core* boundary is a vague concept judged from the way it is used in the literature as it is very model-dependent acquiring values from $\eta \equiv R_{\rm c}/R_\star = 0.2$ (Icke et al. 1992) to $\eta = 0.9$ (Stellingwerf (1986)). The root of this inconsistency may reside in an image of the envelope different in each model. An envelope structure should include, from inner to outer regions: the damping region, the driving region, the transition region and the dissipation region. In our view, the shell participating in the pulsation should include only the dissipation region as all the layers below it are almost in an adiabatic regime and thus do not intervene in the driving.

The formula used in Stellingwerf (1986) assumes an equilibrium value of the form factor and thus allows the shell radius to reach values smaller than the core radius. For the present study, we have used the original formula of Usher & Whitney (1968). We have undergone a parametric study of the $(\gamma_{\rm c}, \zeta, \zeta_{\rm c})$ space for such a case,

as well as an inventory of the subsequent light curve morphology. In the (ζ, ζ_c) plane, the amplitude and the period of the limit cycle increase as one changes the values of the parameters from the stable region to the unstable region, thus the proximity to the latter zone also gives the values of the parameters that yield maximum amplitudes of oscillations. This remark is valid both for the case of constant and variable form factor. The work of Bono et al. (1999) allows us to identify the stable-to-limit-cycle border by the "red edge" of the Cepheid instability strip and the limit-cycle-to-unstable border by its "blue edge". Moreover, this transition gradually transforms the convective luminosity from a sinusoidal variation to a pulse-like variation and also leads to the appearance of a bump-like feature on the ascending branch of the total luminosity. The bump increases as the period of the light curve increases, but for the case of constant form factor, never reaches the height of the main peak which might be considered of radiative origin. The double-peak appearance of the light curves makes a clear reference to what are generally called the Bump Cepheids. For the case of variable form factor, approaching the unstable region through the limit-cycle region leads to the light curve acquiring also a double-peak form, with the first peak gaining more and more amplitude with respect to the second one until the former surpasses the latter. This resembles a reverse Hertzsrpung Progression, with a bump appearing on the ascending branch for shorter periods than for higher ones. However, a direct comparison with the observed periods cannot be made as our time variable is normalized to the dynamical time scale which may be different for different values of the parameters. Nevertheless, it is rewarding to obtain a progression depending on the convection efficiency from a one-zone model and thus maybe help shed some light into the Hertzsrpung progression whose cause is still under debate (Bono et al. 2000b).

In spite of a richer morphology of the limit cycles, the detriment of the variability of the form factor consists in the disappearance of the limit-cycle cases of $\gamma_c = 1$. We have searched for limit cycles cases in the vicinity of $\gamma_c \approx 1$, but found no such case and thus conclude that the variability of the form factor is too strong a driving for such convective cases to present stable oscillations. We have also dwelled on the effect of the shell thickness on the morphology of the limit cycles and confirmed the expectations consisting in a prolongation of the periods for thicker shells.

Another extension of the work of Stellingwerf (1986) was the introduction of the turbulent pressure which is expected to add to the driving mechanism. We have searched for the regions of limit cycles in the parametric space and confirmed an extension of the areas of limit-cycle regions. The morphology of the light curves is significantly poorer than in the previous cases. All limit cycles have an homologous shape — high convective peak followed by a deep minima — and no progression is observed in the light curves. Moreover, the stable and unstable regions in the (ζ, ζ_c) plane allow no clear transition from a "red edge" to a "blue edge". In the view of these results, the impact of the turbulent pressure on the morphology of the limit cycles impoverishes the comparison with the observed shapes of limit cycles and makes us suggest the disregarding of the turbulent pressure in one-zone modeling adopted

here.

Clearly, the study of pulsating stars is not a narrow-minded research as pulsational instabilities are encountered in many phases of stellar evolution and provide information about the evolutive status of the star that would be inaccessible otherwise. The reductionist view of studying the small parts in order to understand the integer has led both to important successes and to serious drawbacks as the pulsating phenomena still presents several "disturbing problems" (Buchler 1998) in spite of the understanding of the consituent phenomena. For a better identification of the roots of these problems, we have intended in the present work to make use of the one-zone model, an approach initiated successfully by Baker (1966). In the spirit of the motto from the beginning of the thesis, we have looked for the advantages and the disadvantages of the one-zone models, as well as their ability to answer well-defined questions. For a better and more precise interpretation of any possible outcome of such models, their possibilities and limitations must be identified and taken into consideration. Our work yielded several interesting behaviors not encountered in any of the previous studies of one-zone models, such as the bursting regimes of the weakly nonadiabatic model and the progression of the convective model. Also, it has supposed the introduction of phenomena previously neglected in equivalent models, such as the turbulent pressure and the variability of the form factor for the model of Stellingwerf (1986). However, due to the inherent reduction of the physical phenomena at work in multiple layers and regimes in the stellar interiors into a one layer for a one-zone approach, some degeneracy might result whose identification is very difficult. This degeneracy might lead to a particular behavior resulting from several one-zone models in which the physical assumptions are reduced in different ways and thus the real root of the behavior of interest might be difficult to untangle. On the other hand, the codes based on the numerical-hydrodynamics approach which has the advantage of the state-of-the-art physical inputs and numerical methods leading to accurate and detailed information about the stellar pulsations, are becoming more and more complex and thus intricate at the moment of discerning the roots and the effects of individual phenomena. In this sense, it is expected that the one-zone approach will still be helpful for clearing some of the remaining "disturbing problems".

Appendix A

Some important aspects of hamiltonian chaos

The purpose of this appendix is to show the reader several well known results of the theory of dynamic systems used throughout the present work. Along the appendix we will use the linear oscillator and the pendulum to introduce most of these results, which will be superficially described. A more detailed description of the material reviewed here can be found in the excellent review of Zaslavsky et al. (1991) and in the references therein, where most of the graphical material can also be found.

Over the last century attention has shifted from the computation of individual orbits toward the qualitative properties of families of orbits. For example, the question of whether a given orbit is stable can only be answered by studying the development of all orbits whose initial conditions are close to those of the orbit being studied. More generally, one can consider all orbits of a given hamiltonian system (that is,which can be described by hamiltonian equations of motion) and ask whether all, or almost all or most or hardly any are stable. More generally still, one can consider all possible hamiltonian functions within some class, and look for the generic or typical behavior of its family of orbits. Finally, one can ask whether a hamiltonian system displays properties which are typical of the wider class of dynamical systems which may be dissipative. Several studies have indeed shown that hamiltonian systems show fundamental physical differences from the non-hamiltonian systems (Sagdeev et al. 1988).

The phase portrait of a hamiltonian system can be chosen as N position coordinates forming a vector q and N conjugate momentum coordinates, p forming an $M = 2N$ dimensional phase space. The dynamics is determined by the Hamiltonian $H(p, q, t)$:

$$\begin{aligned} \frac{dq}{dt} &= +\frac{\partial H}{\partial p} \\ \frac{dp}{dt} &= -\frac{\partial H}{\partial q}. \end{aligned} \tag{A.1}$$

If the hamiltonian has no explicit time dependence, that is, if $H = H(p(t), q(t))$ then H is a constant of the motion which is identified with the energy of the system. The system is said to be conservative. Hamiltonian dynamics is volume preserving according to Liouville theorem

$$\nabla V = \frac{\partial}{\partial p}\frac{dp}{dt} + \frac{\partial}{\partial q}\frac{dq}{dt} = 0, \tag{A.2}$$

which is the key property determining the difference between hamiltonian and dissipative systems, considering that for the latter the volume contracts to zero for sufficiently large times. This, in particular, means that for hamiltonian systems the phase fluid is incompressible. The consequence of this fact is that attractors or repellers do not exist for hamiltonian systems, and, therefore, one is left with the task of understanding the dynamics in the whole phase space. The absence of limit points and limit quantities such as a limit cycles makes the phase portrait of hamiltonian systems less diverse. Nevertheless, it does not lessen their complexity. The introduction of dissipative factors and the asymptotically limited trajectories associated with them makes dissipative systems less sensitive to various small perturbations.

The basis for understanding chaotic phenomena is the concept of local instability. Consider a droplet in the phase space as a set of all the initial states within a certain volume of phase space. A change in the state of the system with time is equivalent to follow the motion of this drop in the phase space. For a conservative system Eq.(A.2) implies that the volume of the droplet will remain constant. Small variations of the shape of the drop correspond to the stable dynamics of the system. However, very strong changes of the shape of the droplet are also possible. Hence, phase points that are arbitrarily close to each other initially can rapidly diverge in the phase space and the droplet quickly loses its regular shape and spreads out in phase space, its boundary acquiring an irregular shape. This is the most important manifestation of local instability of the system. Due to this property, a strong divergence occurs in a finite time. As a result, the information about the initial trajectory is lost and thus irreversibility arises.

The Poisson bracket $\{\}$ of two quantities, A and B, is defined as

$$\{A, B\} = \frac{\partial A}{\partial q}\frac{\partial B}{\partial p} - \frac{\partial A}{\partial p}\frac{\partial B}{\partial q}. \tag{A.3}$$

If a quantity $F(p, q)$ has zero Poisson bracket with the hamiltonian then it is a constant of the motion:

$$\frac{dF}{dt} = \frac{\partial F}{\partial q}\frac{dq}{dt} + \frac{\partial F}{\partial p}\frac{dp}{dt} = \{F, H\} = 0. \tag{A.4}$$

A hamiltonian system with a $2N$ dimensional phase space is said to be integrable if there are N independent constants of motion $F_{\rm m}(p,q)$, $1 \leq m \leq N$ that verify $\{F_{\rm i}, F_{\rm j}\} = 0$. Then the functions $F_{\rm m}(p,q)$ are constant along each trajectory of the system. For a conservative system, one of these constants of motion is the energy — the hamiltonian itself. For this kind of systems the following properties are valid:

1. The trajectories lie on the surface of a N-dimensional invariant torus.
2. The motion is characterized by N frequencies $\omega_i = \omega_i(F_1, ..., F_N)$, $i = 1, ..., N$.
3. The angular variables which determine the coordinates on the surface of the torus satisfy the equations: $\theta_i = \omega_i t + k_i$, $i = 1, ..., N$, where k_i are constants.

During the motion, the trajectory does not leave the surface of the torus. Therefore, the torus is the invariant characteristic of the system. A set of invariant tori corresponds to a set of different values of the integrals $(F_1, ..., F_N)$. Their relative position in the phase space is determined by its dimension. For $N = 2$, the tori corresponding to the different values of the integrals (F_1, F_2) do not intersect each other and, in fact, divide the phase space. For $N > 2$, the tori intersect each other and do not divide the phase space. As these tori are invariant curves, it is possible to introduce more appropriate coordinates for the phase space with the change of variables $(p,q) \rightarrow (I,\theta)$ with $0 \leq \theta \leq 2\pi$, such that I (the action on the torus) defines on which torus is the motion taking place and θ (the angle on the torus) defines the coordinates on the torus. The motion on the torus is thus

$$\frac{dI}{dt} = 0 \tag{A.5}$$

$$\frac{d\theta}{dt} = \omega(I) = \frac{\partial H}{\partial I}. \tag{A.6}$$

These coordinates are called action-angle variables and are widely used mostly in analytical mechanics as they are topologically natural. With these new variables the hamiltonian is only a function on I, $H = H(I)$. For periodic motion with one degree of freedom, the action variables can be related to the original (p,q) variables through

$$I = \frac{1}{2\pi}\oint p\, dq, \tag{A.7}$$

For the linear oscillator the transformation to action-angle variables is:

$$\begin{aligned} q &= (2I/\omega)^{1/2}\cos\theta \\ p &= (2I/\omega)^{1/2}\sin\theta \\ \theta &= \omega_0 t, \end{aligned} \tag{A.8}$$

which leads to $H(I) = \omega_0 I$. Eq.(A.5) reflects the fact that I is also an integral of motion since it is a function only of the integral of motion H, while Eq.(A.6) defines the frequency of the periodic motion $\omega(I)$. The dimensionless parameter

$$\alpha = \frac{I}{\omega}\frac{dI}{d\omega} \tag{A.9}$$

determines the degree of nonlinearity of the system. If $\alpha \neq 0$, the oscillations are called nonlinear and their frequency is a function of energy H. For the linear oscillator, since $H = \omega_0 I$, and $\omega = \omega_0$ is constant, we have $\alpha = 0$, reflecting the linearity of the oscillator.

In an integrable Hamiltonian system, the motion is always periodic or quasiperiodic — geometrically speaking, the orbits move on the tori. Therefore, integrable hamiltonian systems cannot display chaotic behavior. Examples of integrable hamiltonian systems include, for instance, harmonic oscillators (simple mass on a spring or coupled linear springs), the pendulum, or keplerian motion. If the system is nonintegrable, the constraints of the integrals of motion are removed from the trajectories and they move freely through the phase space. Situations in which the integrability of the system is immediately evident or existent are very rare. Far more often, one deals with a problem where a perturbation ϵV is added to an otherwise integrable system, H_0: $H = H_0 + \epsilon V$. In this case, and generally speaking, H will not be integrable for any nonzero ϵ. A large variety of methods exist nowadays to help in analyzing the effects of the perturbation on the system. New methods and techniques have enriched the field of dynamics theory due to the discovery of the dynamic stochasticity or, simply, chaos. Regions of chaos, no matter how small are, imply that the system is, in principle, nonintegrable. It is inherent only to nonlinear systems.

Even if chaos is generic for nonintegrable systems, it has been shown that the trajectories in nonintegrable systems may also be surprisingly stable. Mathematically it consists in the well known theorem of Kolmogorov, Arnold and Moser (KAM). In essence, it says that many of the quasiperiodic motions are preserved under perturbations. These orbits fill out what are called KAM tori. If a KAM torus is perturbed, it reaches a critical stage beyond which quasiperiodic orbits still exist, but instead of tori, they cover Cantor sets. Thus, the transition to chaos in hamiltonian systems can be thought as the destruction of invariant tori and the creation of Cantor sets, as it will be presented in detail below. Chirikov (1979) was the first to realize that this transition to global chaos was an important physical phenomena. Local chaos also occurs in hamiltonian systems (in the region between the different KAM tori) and is

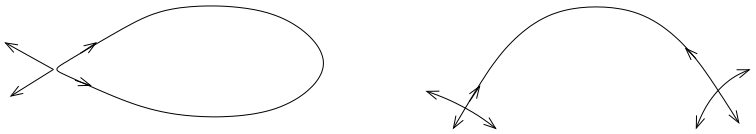

Figure A.1: Homoclinic orbit *(a)* connecting a hyperbolic point to itself and heteroclinic orbit *(b)* connecting two hyperbolic points.

connected with homoclinic or, a in a more general case, heteroclinic orbits, that is to the property of local instability, as it will be illustrated in the examples below.

A.1 The perturbed pendulum

The hamiltonian of the unperturbed nonlinear pendulum has the form:

$$H = \frac{1}{2}\dot{x}^2 - \omega_0^2 \cos x, \tag{A.10}$$

where unit mass is assumed and ω_0 is the frequency of weak oscillations. The fixed points are of the elliptic type, for $x = 2\pi n$, and $\dot{x} = 0$, and saddles, for $x = \pi(2n+1)$, and $\dot{x} = 0$, with $n = 0, \pm 1, \pm 2, ...$ When $H < \omega_0^2$, the trajectories correspond to the oscillations of the pendulum (finite motion), in the case of $H > \omega_0^2$, to rotation of the pendulum (infinite motion). The trajectory with $H = \omega_0^2$ passes through the unstable equilibrium points (saddle or hyperbolic points) and it is called the separatrix, as it defines the border between two distinct classes of orbits: those which correspond to finite motions, and those which correspond to infinite motions. As a general rule, the region of the phase space adjacent to a separatrix is especially sensitive to any disturbance, even to a very weak one. There are two types of separatrices: the heteroclinic ones, which connect distinct fixed points, and the homoclinic ones, which connect a fixed point to itself. Now let us consider a perturbation for the nonlinear pendulum and write the equation of motion as:

$$\ddot{x} + \omega_0^2 \sin x = \epsilon k \omega_0^2 \sin(kx - \nu t), \tag{A.11}$$

with the associated Hamiltonian:

$$H = \frac{1}{2}\dot{x}^2 - \omega_0^2 \cos x + \epsilon \omega_0^2 cos(kx - \nu t). \tag{A.12}$$

The perturbation represents a plane wave that propagates along the x axis at the speed ν/k. This equation is also a common equation in plasma physics and optics as well. Zaslavsky et al. (1991) have shown that for arbitrarily small ϵ in the vicinity of an unperturbed separatrix, a region arises in which the pendulum dynamics becomes stochastic. This region is called stochastic layer. The thickness of the layer increases

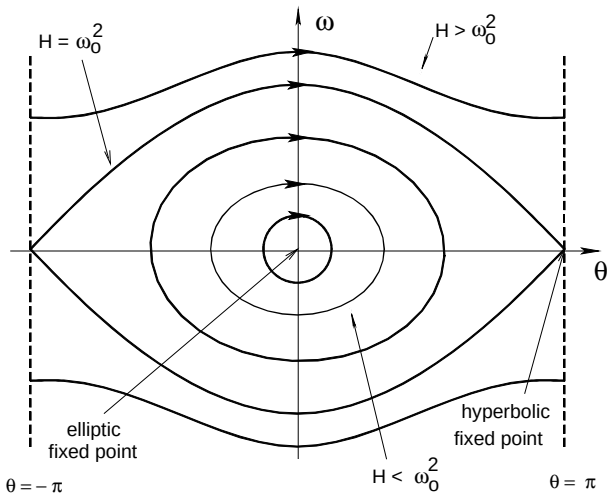

Figure A.2: Phase space of the nonlinear pendulum.

exponentially with ϵ. The existence of the stochastic layer is a universal property of hamiltonian systems. In a typical case many separatrices are present in the phase space. External perturbations destroy the unperturbed separatrices or clothe every one of them in a stochastic layer. Depending on the thickness of the layers and on their positions in the phase space, they can merge into large regions of stochastic dynamics, producing what is called a stochastic sea. Therefore, the stochastic layer can be considered to be a seed for chaos in hamiltonian systems. Any trajectory whose initial condition belongs to the stochastic sea passes through every point of the sea. Therefore, the entire sea can be explored with the help of a single trajectory.

Reconsidering the concept of local instability presented above, if we consider a volume element in the phase space represented as a phase drop and we imagine the phase space outside the drop consisting of another liquid (say of different color), the local instability will give rise to rapid mixing of the two liquids. The ability to explore the whole sea by following only one trajectory is an immediate consequence of the mixing process. However, there are numerous islands, which the chaotic trajectory cannot penetrate. Within an island there are regions of quasiperiodic motion (invariant tori) and regions of trapped chaos. The stronger the chaos, the smaller the islands are and the larger the fraction of the phase space occupied by the stochastic sea.

At this point a more precise introduction to the KAM theory is needed for a better understanding of the fate of the invariant tori for the non-integrable hamiltonian H as ϵ is increased. Considering the frequencies $\omega_i = \partial H/\partial I_i$, with $i = (1, ..., N)$, the condition of non-degeneracy means that the N frequencies ω_i are independent (and, hence, H_0 is nonlinear):

$$\det \left| \frac{\partial \omega_i(I)}{\partial I_j} \right| = \det \left| \frac{\partial^2 H_0}{\partial I_i \partial I_j} \right| \neq 0. \tag{A.13}$$

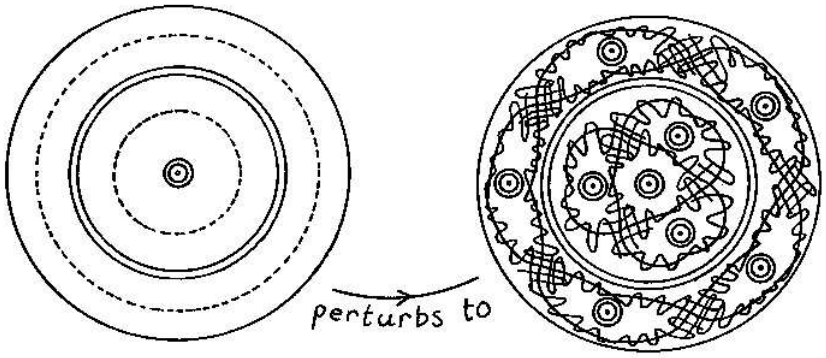

Figure A.3: The breaking of the rational tori — dashed lines — into a sequence of elliptic and hyperbolic fixed points. From Berry (1978).

The KAM theory is associated basically with the problem of conservation of the independent integrals of motion of hamiltonian systems (thus, the invariant tori) in the presence of weak perturbations of the form:

$$H = H_0(I_1, ..., I_N) + \epsilon V(I_1, \theta_1; ...; I_N, \theta_N; t). \tag{A.14}$$

In this case of a time-dependent perturbation with a given angular frequency ν, one can introduce the phase $\theta = \nu t$ into V and increase the number of degrees of freedom of the system with half a degree of freedom due to the perturbation.

The condition of resonance implies that the ratio $\omega(I)/\nu$ must be rational or, more precisely, that there exist values k_0, l_0 and I_0, being k_0 and l_0 integers, such that $k_0\omega_0(I_0) = l_0\nu$, where I_0 defines the resonant torus. The KAM theorem says that if the unperturbed hamiltonian is non-degenerate, then, for a sufficiently small ϵ, most of the non-resonant (irrational) tori will not disappear, but will only undergo a slight deformation, remaining continuous and, hence, unpenetrable for other trajectories. Hence, chaos is impossible in these regions. Rational tori break up into a sequence of elliptic and hyperbolic fixed points (Figure A.3), a behavior that is repeated on finer and finer scales. The islands begin to break up into groups of smaller newborn islands, in a cascade of bifurcations that results in a fractal structure. There is an infinite number of bifurcations and each one globally changes the general structure of the phase space. The sequence of values of the perturbation parameter that corresponds to the bifurcations is characterized by certain regularities. The analysis of these regularities led to the introduction of the renormalization group into the studies of dynamical systems. It is worth noticing at this point that when new islands are born, a new separatrix must also appear to divide them. The very same perturbation that causes the bifurcation and the appearance of the separatrix, brings about its simultaneous breakdown which is accompanied by the creation of the stochastic layer.

The existence of hyperbolic points of Poincaré maps guarantees the existence of chaos. The hyperbolic point in a mapping represents the intersection of a stable (in-

sets) and an unstable manifold (out-sets). The stable and unstable manifolds are the nonlinear extension of the stable and unstable eigenvectors of the linear analysis around the fixed point. This intersection triggers the chaotic behavior in the resulting web called Poincaré heteroclinic structure. At a hyperbolic singularity four curves join, corresponding to the two incoming separatrices (stable manifold), H^+, and the two outcoming separatrices (unstable manifold), H^-.

An important and crucial theorem in the theory of dynamic systems states that if the in-sets and out-sets of a saddle point in the Poincaré map of a dynamical system intersect in one homoclinic structure at a certain point, then there must be an infinite number of homoclinic intersections. The complex manner of oscillation of a trajectory near the saddle point results in what is called homoclinic tangle.

Returning to the discussion on the number of degrees of freedom, for $N = 2$, the destroyed tori lie between the invariant ones because the invariant tori divide the phase space and therefore the trajectory is squeezed between these invariant tori and the variations of the actions are very small. For $N > 2$, the invariant tori no longer divide the phase space, meaning that destruction regions may join and permeate the entire phase space, just like a spider-web often called stochastic web.

Despite the thinness of the stochastic layers, particles can wander along the channels of the newborn web, a phenomenon that represents a universal instability of almost all physical systems with $N > 2$. This global wandering over the phase space for an arbitrary weak perturbation is called minimal chaos. Weak chaos manifests itself in the form of a stochastic layer (for $N > 1$) or a stochastic web (for $N > 2$). These statements also prove that regions of eternal stability exist and that their measure approaches the full volume of phase space as ϵ goes to zero. The theorem also excludes for general hamiltonians the possibility of an absolute chaos in which regular elements are absent. If the system is degenerate, the stochastic web becomes possible even when $N = 3/2$. This dimension is the minimum one because for $N = 1$ dynamic systems are integrable and chaos is impossible. The coexistence of regions of stable dynamics and regions of chaos in the phase space in this system illustrates the difference between chaotic systems and ordinary random processes where no stability islands are present. This property makes possible the analysis of the onset of chaos and the appearance of minimal regions of chaos. Due to the integrability of the system of Eq. (A.14), some important analytic results are available, such as the equation of motion on the separatrix, the width of the stochastic layer and the condition of the onset of local instability (Zaslavsky et al., 1991). In the general case, these characteristics cannot be determined exactly, although some satisfactory estimates are possible.

Nonlinearity plays an exceptional role when the resonance condition between the unperturbed frequency and the perturbation frequency is fulfilled. In the nonlinear case, since the frequency of oscillations is amplitude-dependent, the resonance cannot lead to an unlimited growth of the energy of the system and the resonance becomes mismatched. That is, nonlinearity can rapidly drive the system out of resonance condition and stabilize it.

A.2 The perturbed oscillator

Consider now the motion of a linear oscillator affected by a perturbation in the form of a plane wave:

$$\ddot{x} + \omega_0^2 x = \frac{1}{k}\epsilon\omega_0^2 \sin(kx - \nu t), \tag{A.15}$$

with the associated hamiltonian:

$$H = \frac{1}{2}(\dot{x}^2 + \omega_0^2 x^2) + \frac{1}{k^2}\epsilon\omega^2 \cos(kx - \nu t). \tag{A.16}$$

This problem is equivalent to the motion of a particle in a constant magnetic field and in the field of a plane wave traveling perpendicularly to the magnetic field. Transforming Eq. (A.16) by using the action-angle variables:

$$\begin{aligned} x &= \sqrt{\frac{2I_x}{\omega_0}}\ \sin\phi_x \\ \dot{x} &= \sqrt{2I_x\omega_0}\ \cos\phi_x, \end{aligned} \tag{A.17}$$

one gets

$$\begin{aligned} H &= \omega_0 I_x + \epsilon V(I_x, \phi_x; t) \\ V(I_x, \phi_x; t) &= \frac{1}{k^2}\omega_0^2 \cos\left[k\sqrt{\frac{2I_x}{\omega_0^2}}\sin\phi_x - \nu t\right]. \end{aligned} \tag{A.18}$$

As the unperturbed hamiltonian does not satisfy the non-degeneracy condition, in the case of resonance $n\omega_0 = \nu$, with n integer, the amplitude of the oscillations can largely increase. Thus, only due to the perturbation it is possible to escape from the resonance. Consider the following change of variables in Eq. (A.16):

$$\begin{aligned} x &= \rho\sin\phi \\ \dot{x} &= \omega_0\rho\cos\phi \end{aligned} \tag{A.19}$$

and the expansion:

$$\cos(kx - \nu t) = \cos(k\rho\sin\phi - \nu t) = \sum_{m=-\infty}^{m=+\infty} J_m(k\rho)\cos(m\phi)\cos(m\phi - \nu t), \tag{A.20}$$

where J_m are the Bessel functions. With these new expressions, the hamiltonian becomes:

$$\begin{aligned} H = \frac{1}{2}\omega_0^2\rho^2 &+ \frac{1}{k^2}\epsilon\omega_0^2 J_{n_0}(k\rho)\cos(n_0\phi - \nu t) \\ &+ \frac{1}{k^2}\epsilon\omega_0^2 \sum_{m\neq n_0} J_m(k\rho)\cos(m\phi)\cos(m\phi - \nu t), \end{aligned} \tag{A.21}$$

where the term of resonance $m = n_0$ has been singled out. A second change of variables:

$$\begin{aligned} I &= \frac{\omega_0\rho^2}{2n_0} \\ \theta &= n_0\phi - \nu t \\ \tilde{H} &= H - \nu I \end{aligned} \tag{A.22}$$

leads to

$$\begin{aligned} \tilde{H} &= (n_0\omega_0 - \nu)I + \frac{1}{k^2}\epsilon\omega_0^2 J_{n_0}(k\rho)\cos\theta \\ &+ \frac{1}{k^2}\epsilon\omega_0^2 \sum_{m\neq n_0} J_m(k\rho)\cos\Big[\frac{m}{n_0}\theta - \big(1 - \frac{m}{n_0}\big)\nu t\Big]. \end{aligned} \tag{A.23}$$

The first bracket in Eq. (A.23) is the unperturbed hamiltonian and the second one, is the perturbation. In the case of resonance, $n_0\omega = \nu$, the hamiltonian is proportional to ϵ. Zaslavsky et al. (1991) have demonstrated that even in the case of resonance $\tilde{H}_0(I,\theta)$ can be considered as the unperturbed part of the hamiltonian, while $\tilde{V}(I,\theta;t)$ can be considered as the perturbation. They also have shown that the separatrices form a net on the phase plane (x,p) as a web with a fixed number of n_0 rays and rotational symmetry by an angle $\alpha = 2\pi/n_0$ for even n_0, and with a number of $2n_0$ rays and rotational symmetry by the angle $\alpha = \pi/n_0$ for odd n_0. The fixed points of the system can be found from:

$$\begin{aligned} \frac{\partial\tilde{H}_0}{\partial I} &= 0 \\ \frac{\partial\tilde{H}_0}{\partial\theta} &= 0 \end{aligned} \tag{A.24}$$

and they are a set of hyperbolic points $(\rho_{\rm h}, \theta_{\rm h})$:

$$\begin{aligned} &J_{n_0}(k\rho_{\rm h}) = 0 \\ &\theta_{\rm h} = (2n+1)\pi/2 \end{aligned} \tag{A.25}$$

and elliptic points $(\rho_{\rm e}, \theta_{\rm e})$:

$$\begin{array}{l} J'_{n_0}(k\rho_{\rm e}) = 0 \\ \theta_{\rm h} = n\pi, \end{array} \tag{A.26}$$

where the prime represents the derivative with respect to I. The family of separatrices is formed by the $2n_0$ rays and by circumferences with the radii $\rho_{\rm h}^{(\rm s)}$ crossing them, where $k\rho_{\rm h}^{(\rm s)}$ are radicals of the Bessel function J_{n_0}. Inside these cells of the web, motion occurs along closed-orbits, centered around the elliptic points of the cells.

The existence of this spiderweb-like separatrix network makes possible the radial motion (significant changes in action) as the perturbation $\epsilon \ll 1$ destroys the separatrices and forms channels of finite width, with stochastic dynamics, where a particle can move without restriction. In a realistic situation, the motion is not unbounded as the web channels become narrower with the increase of energy of the particle (i.e., increase in radius), which makes diffusion weaker within them. The degeneracy of the systems makes this kind of diffusion possible, while any radial motion is ruled out in nondegenerate systems.

It should be noted that in the linear case the existence of the web structure is due uniquely to the presence of the perturbation and it always contains stochastic layers. It is generally called weak chaos — the perturbation itself creates the separatrix network at a certain ϵ_0 and then destroys it as ϵ increases by producing channels of stochastic dynamics. In the nonlinear case, the unperturbed hamiltonian H_0 generates the web, while ϵV clothes it in thin stochastic layers. It is called strong chaos. Moreover, the term $\omega_0^2 x$ generates a rotational symmetry of the trajectories on the phase plane. The perturbation possesses a translational symmetry with respect to the shift $x \to x + 2n\pi/k$ (where n is an integer). Under the resonance condition, $n_0\omega = \nu$, the interaction between these symmetries is strong even for small ϵ. The analysis of the geometric properties of the web resulted from this interaction allows one to find which symmetry wins in this competition. Weak chaos can be seen as a compromise between contradictory symmetries.

Another important relation that can be obtained regards the time derivative of the energy:

$$\dot{H}_0(\dot{x}, x) = \{H, H_0\} = \epsilon\{H_0, V\} = -\epsilon\frac{\partial H_0}{\partial \dot{x}}\frac{\partial V}{\partial x} = -\epsilon\dot{x}\frac{\partial V}{\partial x} \tag{A.27}$$

where $\{\}$ are the Poisson brackets previously defined in this appendix. Therefore, we have

$$\dot{E} = \dot{H}_0 = \epsilon\frac{\omega_0^2}{k}\dot{x}\sin(kx - \nu t) \tag{A.28}$$

Using this equation and the hamiltonian in the form of Eq. (A.21), in the case of resonance the width of the stochastic web was obtained by Zaslavsky (1998) as:

$$\Delta H_{\rm s} = \sqrt{2}\,\pi^{7/2}\frac{1}{\epsilon}(k\rho_0)^{1/2}\frac{\omega_0^2}{k^2}\exp\left\{-\frac{1}{\epsilon}\Big(\frac{\pi}{2}\Big)^{5/2}\sqrt{k\rho_0}\right\} \tag{A.29}$$

where $\rho_0 = (2n_0 I_0/\omega_0)^{1/2}$ and I_0 define the resonant invariant curve. It illustrates that the width of the web decreases quickly as the radius ρ_0 grows, that is, the width of the web for fairly distant cells is exponentially small.

A strong degeneracy can be removed in two ways: by detuning the resonance (that is $n_0\omega \neq \nu$) or by the introduction of a nonlinearity in the unperturbed hamiltonian of Eq (A.16). A similar analysis of the perturbed nonlinear pendulum discussed above performed by Zaslavsky et al. (1991) lead to following terms in the hamiltonian using the notation from Eq. (A.23):

$$\begin{aligned}
\tilde{H}_0(I,\theta) &= (n_0\omega_0 - \nu)I + aI^2 + \frac{1}{k^2}\epsilon\omega_0^2 J_{n_0}(k\rho)\cos\theta \\
\tilde{V}(I,\theta;t) &= \frac{1}{k^2}\epsilon\omega_0^2\sum_{m\neq n_0} J_m(k\rho)\cos\left[\frac{m}{n_0}\theta - \Big(1-\frac{m}{n_0}\Big)\nu t\right],
\end{aligned} \tag{A.30}$$

where the two terms added in $\tilde{H}_0(I,\theta)$ are due to the detuning of the resonance (the former) and to the nonlinearity of the oscillator (the latter). Since the frequency $\delta\omega \neq 0$ when $\epsilon = 0$, or, more exactly

$$\delta\omega \equiv \frac{\partial\tilde{H}_0(I,\theta;\epsilon=0)}{\partial I} = (n_0\omega_0 - \nu) + 2aI \equiv \delta\omega_{\rm R} + \delta\omega_{\rm N} \tag{A.31}$$

the phase portrait of the system in the case of $\tilde{V} = 0$ has no web: degeneracy is taken off. That is, in the phase space there appear invariant curves (deformed tori) embracing the center which do not allow diffusion in the radial direction. The portrait closely resembles a web because, if the perturbation is large enough so that the resulting stochastic layer is wide enough to cover the gaps between separatrices, then a single large web can appear. The greater the value of k, the smaller the cells of the web are (their size is typically of the order of $2\pi/k$). The greater the value of ϵ is, the wider the stochastic web is. In the process of deformation of the KAM-tori, new smaller cells of web-tori are formed as the parameter k is increased. These changes are called KAM-tori to web-tori transition. During this transition there occur an infinite number of bifurcations in the phase space.

Appendix B

Numerical aspects

The present thesis has been devoted to the study of non-linear pulsations of Mira stars. Its main approach is numerical and thus the simulations play the most important role in the subsequent conclusions drawn from the obtained results. Thus, a short review of the numerical aspects and methods used throughout the work is included in this Appendix.

The first dynamical behavior whose numerical implications determine crucially its existence is the stickiness behavior observed for the adiabatic one-zone model in Chapter 3. In Figure 3.16, we represented the variations of radius and velocity as a function of time for a particular choice of the parameters of the system. The behavior consisted in a quiet phase of quasi-periodic oscillations followed by an extremely violent and chaotic phase. One may undoubtely attribute such dynamics to a phenomenon of error propagation and thus, without any physical relevance. To clarify this matter, we have undergone a study concerning the results provided for this particular case by using several methods of numerical integration. As already mentioned in §3.2, we have used for general purpose the fifth order Runge-Kutta integrator with stepsize control and dense output using the Prince-Dormand coefficients (DOPRI method) from Hairer et al. (1993) as well as the code described in Shampine & Gordon (1975). As far as the stickiness property is concerned, it is possible that different integrators produce different trajectories in the phase space (or in the Poincaré map, as in our case) as different tolerances and integration methods are used. This question is even most important in the cases in which one deals with a chaotic trajectory. However, in the analysis of any chaotic system, what is relevant to the dynamics is the phase space — the global features — and not the individual time-evolutions as they might differ due to one of the requisites of chaotic dynamics: the sensitivity to initial conditions. Therefore, in the case of the stickiness, what should be observed with any integrator is the quiet phase followed by a chaotic one, while the phase space presents the same global features. In order to verify this statement, we have used the integrator code from Hairer et al. (1993) with different orders of the Runge-Kutta method and with different absolute and relative tolerances for the integration of Eq. (3.8) with the initial condition of the sticky orbit from Figure 3.16.

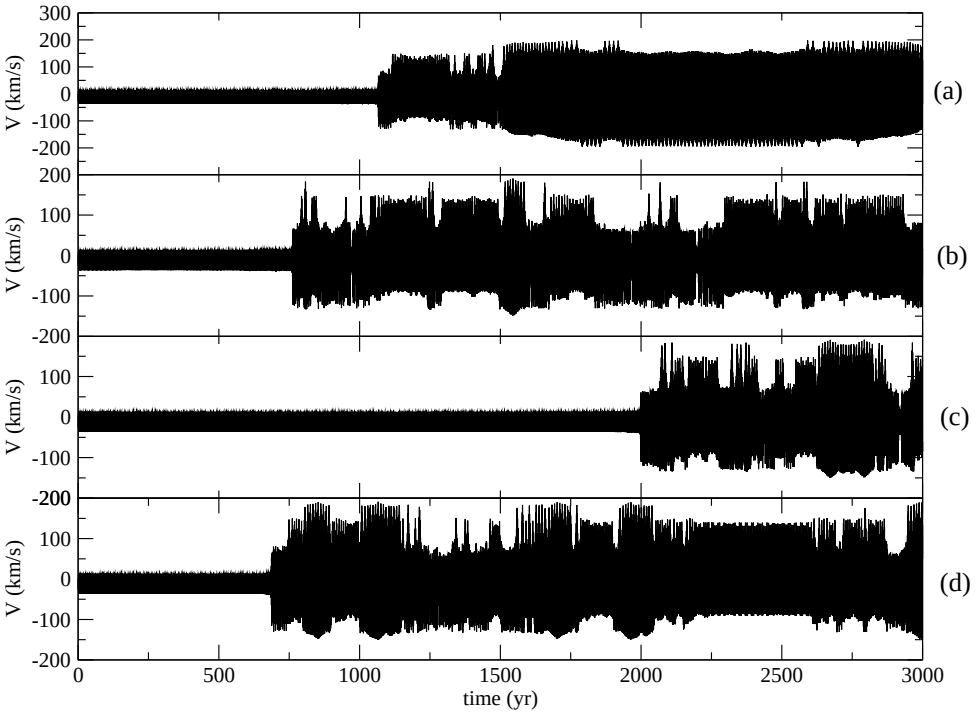

Figure B.1: Variations of velocity as a function of time for $\omega = 3.0146$, $\alpha = 0.3$, $\epsilon = 0.5$ and the initial condition $(x_0, y_0) = (0.0, 0.02)$ and different characteristics of the integration: *(a)* Runge-Kutta of order 8 with double precision and relative and absolute tolerances equal to $10^{-}10$; *(b)* Runge-Kutta of order 5 with quadruple precision and relative and absolute tolerances equal to $10^{-}12$; *(c)* Runge-Kutta of order 8 with quadruple precision and relative and absolute tolerances $10^{-}12$; *(d)* Runge-Kutta of order 8 with quadruple precision and relative and absolute tolerances $10^{-}14$. See text for more details.

The variations of velocity as a function of time sampled for the Poincaré map appear in Figure B.1. The Poincaré map for all cases are equivalent to the Figure 3.17*b* and thus we have chosen not to add it here. Additionally, we have used for this verification the integration code of an implementation of a Runge-Kutta-Fehlberg method of order 8 kindly provided by the Department of Applied Mathematics of the Politechnic University of Catalonia. The results confirmed the behavior typical for a sticky orbit. As the duration of the quiet phase for this case is slightly longer than the time-interval represented in Figure B.1, we have chosen not to add it to the Figure. Moreover, this choice was motivated also by the fact that the calculations leading to the results of Chapter 3 were obtained with the code from Hairer et al. (1993).

For the calculations regarding our weakly nonadiabatic model (Chapter 4) and the convective model (Chapter 5) we have used the codes available from the GNU Scientific Library (GSL) of C and C++ software [1]. More precisely, we have in-

[1] `http://www.gnu.org/software/gsl/`

tegrated all the differential equations using the embedded 8^{th} order Runge-Kutta Prince-Dormand method with 9^{th} order error estimate.

Appendix C

Some astrophysical units and notations

Solar luminosity	$L_\odot = 3.9 \times 10^{26} = 3.9 \times 10^{33}$ erg s^{-1}
Solar mass	$M_\odot = 1.989 \times 10^{30}$ kg
Solar radius	$R_\odot = 6.96 \times 10^{8}$ m
Parsec	1 pc = 3.09×10^{16} m

Magnitude

The quantity L denotes the energy a star radiates per second integrated over all wavelengths and is known as the (bolometric) luminosity. The corresponding bolometric flux of radiation at the earth, F is then given by

$$F = \frac{L}{4\pi d^{\,2}},$$

where d is the distance to the star. The magnitude system for comparing stellar brightnesses is defined by the formula

$$m = -2.5\ \log_{10}\ F + \text{constant},$$

where the factor -2.5 and the value of the constant are chosen to approximate the scale to the magnitude system introduced by Hipparchus in the first century BC. From the definition, it follows that a difference of 5 magnitudes is a factor of 100 in intensity and the smaller or more negative magnitude, the brighter the star. In other words the difference in magnitudes relates directly to the ratio of apparent fluxes: $m_1 - m_2 = -2.5\ \log_{10}\ (F_1/F_2)$.

The bolometric magnitude of a star is defined via

$$m_{\text{bol}} = -2.5\ \log_{10}\ L + 5\ \log_{10}\ d + \text{constant}.$$

It measures the apparent brightness of a star and it is therefore termed the apparent magnitude as it is a function of the star's distance. A lowercase m is always used

to represent an apparent magnitude. The absolute bolometric magnitude $M_{\rm bol}$ is defined to be the apparent bolometric magnitude a star would have if it were at a standard distance taken to be 10 parsecs and hence is given by

$$M_{\rm bol} = -2.5\ \log_{10}\ L + 5 + \text{constant}.$$

Due to the general use of filters in astronomical observations, the magnitude system is effected by the use of notations such as $M_{\rm V}$, $M_{\rm B}$, $M_{\rm U}$ for the absolute magnitude, where V stands for visual, B for blue and U for ultraviolet.

Bibliography

Auvergne, M. & Baglin, A., 1985. A dynamical instability as a driving mechanism for stellar oscillations. *A&A*, **142**, 388–392.

Baker, N., 1966. Simplified models for Cepheid instability. In *"Stellar evolution", Eds. Stein, R.F. & Cameron, A.G.W.* , p. 333. New York: Plenum Press.

Baker, N. & Kippenhahn, R., 1962. The Pulsations of Models of δ Cephei Stars. With 17 Figures in the Text. *Zeitschrift fur Astrophysics*, **54**, 114–151.

Baker, N. H., Moore, D. W. & Spiegel, E. A., 1971. Aperiodic behaviour of a non-linear oscillator. *Quarterly Journal of Mechanics and Applied Mathematics*, **24**, 391–422.

Balmforth, N. J. & Craster, R. V., 1997. Synchronizing Moore and Spiegel. *Chaos*, **7**, 738–752.

Barthes, D. & Mattei, J. A., 1997. Time-Frequency Analysis and Pulsation Modes of LPV Stars.I. omicron Ceti. *AJ*, **113**, 373–390.

Bedding, T. R., Zijlstra, A. A., Jones, A. & Foster, G., 1998. Mode switching in the nearby Mira-like variable R Doradus. *MNRAS*, **301**, 1073–1082.

Benz, W., 1991. An Introduction to Computational Methods in Hydrodynamics. In *"Late Stages of Stellar Evolution. Computational Methods in Astrophysical Hydrodynamics"*, p. 259. Dordrecht: Kluwer Academic Publishers.

Berry, M. V., 1978. Regular and irregular motion. In *"Topics in nonlinear dynamics: A tribute to Sir Edward Bullard"*, 16–120. New York: American Institute of Physics.

Bono, G., Castellani, V. & Marconi, M., 2000a. Classical cepheid pulsation models. III. The predictable scenario. *ApJ*, **529**, 293–317.

Bono, G., Marconi, M. & Stellingwerf, R. F., 1999. Classical cepheid pulsation models. I. Physical structure. *ApJS*, **122**, 167–205.

Bono, G., Marconi, M. & Stellingwerf, R. F., 2000b. Classical Cepheid pulsation models — VI. The Hertzsprung progression. *A&A*, **360**, 245–262.

Bono, G. & Stellingwerf, R. F., 1994. Pulsation and stability of RR Lyrae stars. 1: Instability strip. *ApJS*, **93**, 233–269.

Bowen, G. H., 1988. Dynamical modeling of long-period variable star atmospheres. *ApJ*, **329**, 299–317.

Buchler, J. R., 1993. A dynamical systems approach to nonlinear stellar pulsations. *Ap&SS*, **210**, 9–31.

Buchler, J. R., 1998. Nonlinear Pulsations. In *"A Half Century of Stellar Pulsation Interpretation: A Tribute to Arthur N. Cox", Eds. Bradley, P.A. & Guzik, J. A., ASP Conf. Ser. Vol. 135*, p. 220.

Buchler, J. R. & Goupil, M.-J., 1988. A mechanism for the irregular variability of supergiant stars. *A&A*, **190**, 137–147.

Buchler, J. R. & Kolláth, Z., 2001. Nonlinear analysis of irregular variables. In *"Stellar pulsation – Nonlinear Studies", Eds. Takeuti, M. & Sasselov, D.D.*, p. 185. Dordrecht: Kluwer Academic Publishers.

Buchler, J. R., Kolláth, Z. & Cadmus, R., 2002. Chaos in the Music of the Spheres. In *"Experimental Chaos", AIP Conf. Proc. Vol. 622*, p. 61.

Buchler, J. R., Perdang, J. M. & Spiegel, E. A., eds., 1985. *"Chaos in astrophysics"*. NATO ASIC Proc. 161: Compendium in Astronomy.

Buchler, J. R. & Regev, O., 1982. Oscillations of an extended ionization region in a star. *ApJ*, **263**, 312–319.

Buchler, J. R., Serre, T., Kolláth, Z. & Mattei, J., 1995. A chaotic pulsating star: The case of R Scuti. *Phys. Rev. Lett.*, **74**, 842–845.

Buchler, J. R., Yueh, W. R. & Perdang, J., 1977. Two-time method applied to a one-zone atmosphere. *ApJ*, **214**, 510–521.

Carroll, B. W. & Ostlie, D. A., 1996. *"An introduction to modern astrophysics"*. Reading, MA: Addison–Wesley.

Castor, J. I., 1971. On the Calculation of Linear, Nonadiabatic Pulsations of Stellar Models. *ApJ*, **166**, 109–130.

Chirikov, B., 1979. A universal instability of manydimensional oscillator systems. *Physics Reports*, **52**, 263–370.

Choi, H. & Williams, W., 1989. Improved time-frequency representation of multi-component signals using exponential kernels. *IEEE Trans. ASSP*, **37**, 862–871.

CHRISTENSEN-DALSGAARD, J., 2003. *"Lecture Notes on Stellar Oscillations"*. Electronic book available at `http://astro.phys.au.dk/~jcd/oscilnotes/`.

CLEMENT, C. C., DICKENS, R. J. & BINGHAM, E. E., 1979. The RR Lyrae variable stars in the globular cluster IC 4499. *AJ*, **84**, 217–230.

COHEN, L., 1966. Generalized phase-space distribution functions. *J. Math. Phys.*, **7**, 781–806.

COHEN, L., 1995. *"Time-frequency analysis"*. Englewood Cliffs, NJ: Prentice Hall.

CONTOPOULOS, G., 1971. Orbits in Highly Perturbed Dynamical Systems. Nonperiodic Orbits. *AJ*, **76**, 147–156.

COVAS, E. O., 1995. *"Nonlinear dynamics in astrophysics"*. M.Sc. Thesis, Queen Mary & Westfield College.

COX, A. N., 2003. A Pulsation Mechanism for GW Virginis Variables. *ApJ*, **585**, 975–982.

COX, A. N. & OSTLIE, D. A., 1993. A linear and nonlinear study of Mira. *Ap&SS*, **210**, 311–319.

COX, J. P., 1980. *"Theory of stellar pulsation"*. Princenton, NJ: Princeton University Press.

DE LOORE, C. & DOOM, C., 1992. *"Structure and evolution of single and binary stars", Ap&SS Library Vol. 179*. Dordrecht: Kluwer Academic Publishers.

DEL CASTILLO NEGRETE, D. & FIRPO, M., 2002. Coherent structures and self-consistent transport in a mean field Hamiltonian mode. *Chaos*, **12**, 496–507.

DEL CASTILLO NEGRETE, D., GREENE, J. M. & MORRISON, P. J., 1996. Area preserving nontwist maps: periodic orbits and transition to chaos. *Physica D*, **91**, 1–23.

DEL CASTILLO NEGRETE, D., GREENE, J. M. & MORRISON, P. J., 1997. Renormalization and transition to chaos in area preserving nontwist maps. *Physica D*, **100**, 311–329.

DULLIN, H. R., MEISS, J. D. & STERLING, D., 2000. Generic twistless bifurcations. *Nonlinearity*, **13**, 203–224.

EDDINGTON, A. S., 1917. The pulsation theory of Cepheid variables . *The Observatory*, **40**, 290–293.

EDDINGTON, A. S., 1919. On the pulsations of a gaseous star. *MNRAS*, **79**, 177–199.

FEAST, M. W., GLASS, I. S., WHITELOCK, P. A. & CATCHPOLE, R. M., 1989. A period-luminosity-colour relation for Mira variables. *MNRAS*, **241**, 375–392.

FEUCHTINGER, M. U., 1999. A nonlinear convective model for radial stellar pulsations. I. The physical description. *A&AS*, **136**, 217–226.

FLEISCHER, A. J., GAUGER, A. & SEDLMAYR, E., 1995. Circumstellar dust shells around long-period variables. III. Instability due to an exterior {kappa}-mechanism caused by dust formation. *A&A*, **297**, 543–555.

GÁBOR, D., 1946. Theory of communication. *J. Inst. Elec. Eng.*, **93**, 429–457.

GARCIA-BERRO, E., RITOSSA, C. & IBEN, I. J., 1997. On the Evolution of Stars That Form Electron-Degenerate Cores Processed by Carbon Burning. III. The Inward Propagation of a Carbon-burning Flame and Other Properties of a 9 $M_{\odot}$ Model Star. *ApJ*, **485**, 765–784.

GAUTSCHY, A., 1997. The development of the theory of stellar pulsations. *Vistas in Astronomy*, **41**, 95–115.

GAUTSCHY, A. & GLATZEL, W., 1990. On Highly Non-Adiabatic Stellar Pulsations and the Origin of Strange Modes. *MNRAS*, **245**, 597–613.

GAUTSCHY, A. & SAIO, H., 1995. Stellar Pulsations Across The HR Diagram: Part 1. *ARA&A*, **33**, 75–114.

GOUGH, D. O., 1967. Convection in Pulsating Stars: Time-Dependent Mixing-Length Theory in the One-Zone Model. *AJ*, **72**, 799–800.

GOUPIL, M. J., AUVERGNE, M. & BAGLIN, A., 1991. Wavelet analysis of pulsating white dwarfs. *A&A*, **250**, 89–98.

GUCKENHEIMER, J. & HOLMES, P., 1993. *"Nonlinear oscillations, dynamical systems and bifurcations of vector fields"*. Heidelberg: Springer–Verlag.

HÖFNER, S., 1999. A new generation of dynamic model atmospheres for AGB stars: first results. *A&A*, **346**, L9–L12.

HÖFNER, S., GAUTSCHY-LOIDL, R., ARINGER, B. & JØRGENSEN, U. G., 2003. Dynamic model atmospheres of AGB stars. III. Effects of frequency-dependent radiative transfer. *A&A*, **399**, 589–601.

HAIRER, E., NORSETT, S. & WANNER, G., 1993. *"Solving Ordinary Differential Equations I. Nonstiff Problems", Springer–Verlag Ser. in Comp. Math.*. Heidelberg: Springer–Verlag.

HAWKINS, G., MATTEI, J. A. & FOSTER, G., 2001. R Centauri: An Unusual Mira Variable in a He-Shell Flash. *PASP*, **113**, 501–506.

HJORTH, P. G., VILLEMOES, L. F., TEUBER, J. & FLORENTIN-NIELSEN, R., 1992. Wavelet analysis of 'double quasar' flux data. *A&A*, **255**, L20–L23.

Hoefner, S., Jorgensen, U. G., Loidl, R. & Aringer, B., 1998. Dynamic model atmospheres of AGB stars. I. Atmospheric structure and dynamics. *A&A*, **340**, 497–507.

Howard, J. & Humpherys, J., 1995. Nonmonotonic Twist Maps. *Physica D*, **80**, 256–276.

Icke, V., Frank, A. & Heske, A., 1992. Weak chaos in long-period variables. *A&A*, **258**, 341–356.

Iooss, G. & Joseph, D. D., 1990. *"Elementary stability and bifurcation theory"*. Heidelberg: Springer–Verlag.

Kiss, L. L. & Szatmáry, K., 2002. Period-doubling events in the light curve of R Cygni: Evidence for chaotic behaviour. *A&A*, **390**, 585–596.

Kolláth, Z. & Buchler, J. R., 1997. Time-Frequency Analysis of Variable Star Light Curves. In *"Nonlinear Signal and Image Analysis", Eds. Buchler, J.R. & Kandrup, H., Vol. 808*, p. 116. New York: New York Academy of Sciences.

Kolláth, Z. & Buchler, J. R., 2001. Double-mode stellar pulsations. In *"Stellar pulsation – Nonlinear Studies", Eds. Takeuti, M. & Sasselov, D.D.*, p. 29. Dordrecht: Kluwer Academic Publishers.

Kolláth, Z., Buchler, J. R., Serre, T. & Mattei, J., 1998. Analysis of the irregular pulsations of AC Herculis. *A&A*, **329**, 147–154.

Kovács, G. & Buchler, J. R., 1988. Regular and irregular nonlinear pulsation in population II Cepheid models. *ApJ*, **334**, 971–994.

Ledoux, P. & Walraven, T., 1958. Variable Stars. *Handbuch der Physik*, **51**, 353–604.

Lieberman, M. & Lichtenberg, A., 1992. *"Regular and Chaotic Dynamics", Applied Mathematical Sciences, Vol 38*. Heidelberg: Springer–Verlag.

Malatesta, K., 2002. *Variable star of the Month: X Cygni*. AAVSO Archives: http://www.aavso.org/vstar/vsots/0902.shtml.

Mantegazza, L., 1996. BS Lyrae: a double mode Mira star with a dominant first overtone mode. *A&A*, **315**, 481–484.

Meiss, J. D., 1992. Symplectic maps, variational principles, and transport. *Rev. of Mod. Phys.*, **64**, 795–848.

Moore, D. W. & Spiegel, E. A., 1966. A Thermally Excited Non-Linear Oscillator. *ApJ*, **143**, 871–887.

Munteanu, A., García–Berro, E. & José, J., 2003a. Bursting oscillations in long-period variables. In *"Interplay of Periodic, Cyclic and Stochastic Variability in Selected Areas of the H-R Diagram", ASP Conf. Ser. Vol. 292*, 285–291.

Munteanu, A., García–Berro, E. & José, J., 2003b. A weakly non-adiabatic one-zone model of stellar pulsations: application to Mira stars. *MNRAS*, **341**, 855–862.

Munteanu, A., García–Berro, E., José, J. & Petrisor, E., 2002. Complex dynamics in a simple model of pulsations for super-asymptotic giant branch stars. *Chaos*, **12**, 332–343.

Munteanu, A. Petrisor, E., García–Berro, E. & José, J., 2003c. Creation of twistless circles in a model of stellar pulsations. *Communications in Nonlinear Science and Numerical Simulation*, **8**, 355–373.

Norris, J. P., Nemiroff, R. J., Scargle, J. D., Kouveliotou, C., Fishman, G. J., Meegan, C. A., Paciesas, W. S. & Bonnel, J. T., 1994. Detection of signature consistent with cosmological time dilation in gamma-ray bursts. *ApJ*, **424**, 540–545.

Ostlie, D. A. & Cox, A. N., 1986. Luminosity Variation in the One-Zone Cepheid Model. *A&A*, **311**, 864–872.

Pesnell, W. D., 1985. On one-zone models of stellar pulsation. *ApJ*, **299**, 161–166.

Petersen, J. O., 1984. Studies of Cepheid type variability. II - Fourier description of RR Lyrae variables in the globular cluster Omega Centauri. *A&A*, **139**, 496–506.

Petrisor, E., 2001. Nontwist Area Preserving Maps with Reversing Symmetry Group. *Int. J. Bif. & Chaos*, **11**, 497–511.

Rudd, T. J. & Rosenberg, R. M., 1970. A simple model for cepheid variability. *A&A*, **6**, 193–205.

Sagdeev, R. Z., Usikov, D. A. & Zaslavsky, G. M., 1988. *Nonlinear physics. From the pendulum to turbulence and chaos.* Contemporary Concepts in Physics, New York: Harwood Academic Publishers.

Saitou, M., Takeuti, M. & Tanaka, Y., 1989. Chaotic behavior in nonlinear radial oscillations of one-zone stellar models. *PASJ*, **41**, 297–309.

Saitou, S., Nomura, Y., Hirose, K. & Ichikawa, Y., 1997. Separatrix reconnection and periodic orbit annihilation in the Harper map. *Chaos*, **7**, 245–253.

Sanders, J. & Verhulst, F., 1985. *"Averaging methods in nonlinear dynamical systems"*. Heidelberg: Springer–Verlag.

Schatzman, E. L., Praderie, F. & King, A. R., 1993. *"The Stars"*. Berlin: Springer-Verlag.

Serre, T., Kollath, Z. & Buchler, J. R., 1996a. Search for low-dimensional nonlinear behavior in irregular variable stars. The analysis of irregular W Virginis model pulsations. *A&A*, **311**, 845–851.

Serre, T., Kollath, Z. & Buchler, J. R., 1996b. Search for low-dimensional nonlinear behavior in irregular variable stars. The global flow reconstruction method. *A&A*, **311**, 833–844.

Shampine, L. & Gordon, M., 1975. *"Computer Solution of Ordinary Differential Equations: The Initial Value Problem"*. San Francisco, CA: W.H. Freeman & Co.

Shirts, R. B. & Reinhardt, W. P., 1982. Approximate constants of motion for classically chaotic vibrational dynamics - Vague tori, semiclassical quantization, and classical intramolecular energy flow. *J. Ch. Ph.*, **77**, 5204–5217.

Simis, Y., 2001. *" Mass loss modulation in dust forming stellar winds"*. PhD Thesis, Leiden University.

Simó, C., 1998. Invariant curves of analytic perturbed nontwist area preserving maps. *Regular & Chaotic Dynamics*, **3**, 180–195.

Slezak, E., Durret, F. & Gerbal, D., 1994. A wavelet analysis search for substructures in eleven X-ray clusters of galaxies. *AJ*, **108**, 1996–2008.

Stellingwerf, R. F., 1972. Luminosity Variation in the One-Zone Cepheid Model. *A&A*, **21**, 91–96.

Stellingwerf, R. F., 1979. Pulsation in the lower Cepheid strip. I - Linear survey. *ApJ*, **227**, 935–942.

Stellingwerf, R. F., 1982. Convection in pulsating stars. I - Nonlinear hydrodynamics. II - RR Lyrae convection and stability. *ApJ*, **262**, 330–343.

Stellingwerf, R. F., 1986. Luminosity Variation in the One-Zone Cepheid Model. *A&A*, **303**, 119–129 (S86).

Stellingwerf, R. F. & Donohoe, M., 1986. Fourier coefficients of variable stars. *ApJ*, **306**, 183–198.

Stellingwerf, R. F. & Donohoe, M., 1987. Fourier coefficients of variable stars. II - Light-curve analysis. *ApJ*, **314**, 252–260.

Stellingwerf, R. F. & Gautschy, A., 1988. The effects of radiation pressure on stellar stability. *ApJ*, **327**, 801–808.

Stellingwerf, R. F., Gautschy, A. & Dickens, R. J., 1987. Overtone pulsation in stars. *ApJ*, **313**, L75–L79.

Stobie, R. S. & Whitelock, P. A., eds., 1995. *Astrophysical applications of stellar pulsation*. ASP Conf. Ser. 83: IAU Colloq. 155.

Strogatz, S., 1994. *"Nonlinear Dynamics and Chaos with applications to Physics, Biology, Chemistry, and Engineering"*. Reading, MA: Addison–Wesley.

Takeuti, M., 1990. Regular and Irregular Pulsations. In *"Numerical Modelling of Nonlinear Stellar Pulsations: Problems and Prospects"*, 121–141.

Takeuti, M. & Buchler, J. R., eds., 1993. *"Nonlinear phenomena in stellar variability"*. Dordrecht: Kluwer Academic Publishers, Ap&SS Vol. 210, (IAU Colloq. 134).

Tanaka, Y. & Takeuti, M., 1988. A model oscillator of irregular stellar variability. *Ap&SS*, **148**, 229–237.

Unno, W. & Xiong, D.-R., 1993. One zone modeling of irregular variability of stellar convective envelope. *Ap&SS*, **210**, 77–81.

Usher, P. D. & Whitney, C. A., 1968. Non-Linear Pulsations of Discrete Stellar Models. I. First-Order Asymptotic Theory of the One-Zone Model. *ApJ*, **154**, 203–214.

Van der Weele, J. P. & Valkering, T. P., 1990. The birth process of periodic orbits in non-twist maps. *Physica A*, **169**, 42–72.

Van Horn, H. M., Thomas, J. H., Frank, A. & Blackman, E. G., 2003. Fuel-Supply-limited Stellar Relaxation Oscillations: Application to Multiple Rings around Asymptotic Giant Branch Stars and Planetary Nebulae. *ApJ*, **585**, 983–992.

Vassiliadis, E. & Wood, P. R., 1993. Evolution of low- and intermediate-mass stars to the end of the asymptotic giant branch with mass loss. *ApJ*, **413**, 641–657.

Wood, P. R., 2000. Convection-Induced Oscillatory Thermal Modes in Red Giants: A New Type of Stellar Oscillation. In *ASP Conf. Ser. 203:The Impact of Large-Scale Surveys on Pulsating Star Research*, 379–380.

Wood, P. R., Alcock, C., Allsman, R. A., Alves, D., Axelrod, T. S. et al., 1999. MACHO observations of LMC red giants: Mira and semi-regular pulsators, and contact and semi-detached binaries. In *IAU Symp. 191: Asymptotic Giant Branch Stars*, 151–158.

Xiong, D. R., Cheng, Q. L. & Deng, L., 1998b. Turbulent Convection and Pulsational Stability of Variable Stars. II. Oscillations of RR Lyrae and Horizontal Branch Red Variable Stars. *ApJ*, **500**, 449–465.

Xiong, D. R. & Deng, L., 2001. Turbulent convection and pulsational stability of variable stars - IV. The red edge of the δ Scuti instability strip. *MNRAS*, **324**, 243–248.

Xiong, D. R., Deng, L. & Cheng, Q. L., 1998a. Turbulent Convection and Pulsational Stability of Variable Stars. I. Oscillations of Long-Period Variables. *ApJ*, **499**, 355–366.

Ya'ari, A. & Tuchman, Y., 1996. Long-Term Nonlinear Thermal Effects in the Pulsation of Mira Variables. *ApJ*, **456**, 350–355.

Yao, B., Zhang, C., Qin, D. & Tong, J., 1993. Low amplitude new type variable stars in globular clusters. *Ap&SS*, **210**, 163–165.

Zaslavsky, G., 1998. *"Physics of Chaos in Hamiltonian Dynamics"*. London: Imperial College Press.

Zaslavsky, G., Sagdeev, R., Usikov, D. & Chemikov, A., 1991. *"Weak Chaos and Quasiregular Structures"*. Cambridge: Cambridge University Press.

Zaslavsky, G. M., 1999. Chaotic dynamics and the origin of statistical laws. *Phys. Today*, **52**, 39–45.

Zaslavsky, G. M., 2002. Dynamical traps. *Physica D*, **168**, 292–304.

Zhevakin, S. A., 1963. Physical Basis of the Pulsation Theory of Variable Stars. *ARA&A*, **1**, 367–400.

Zijlstra, A. A., Loup, C., Waters, L. B. F. M., Whitelock, P. A., van Loon, J. T. & Guglielmo, F., 1996. Obscured asymptotic giant branch stars in the Magellanic Clouds - II. Near-infrared and mid-infrared counterparts. *MNRAS*, **279**, 32–62.